

**“Large Scale Physical Modelling Study of a Flexible Barrier under the Impact of Granular Flows” (nhess-2018-131)**

**Reply to Review Comments from the Editor**

**by Dao-yuan TAN and Co-Authors**

The authors wish to thank the handling editor for his insightful and constructive comments on the manuscript and advice to us for improving the quality of the draft paper. The authors have taken full consideration of all those comments and made clarification and corrections in following tables:

No.	Editor’s comments	Reply
1	Thank you for your response, please address the comments of the reviewers in an updated version.	Reply: Thank you for your reminder, all the comments of the reviewers and corresponding revisions have been addressed in the updated version in the attached files using black underlined fonts.
2	Very important that you address the issues of the Cd (drag coefficient) as I think most practicing engineers are interested in this value. Please note that a recent paper has been published in this field in the Canadian Geotechnical Journal: <a href="https://doi.org/10.1139/cgj-2016-0157">https://doi.org/10.1139/cgj-2016-0157</a> .	Reply: This suggestion is very valuable and helpful to improve the draft: nhess-2018-131. The published paper by Wendeler <i>et al.</i> (2018) reviewed previous laboratory tests (Wendeler and Volkwein 2015) and full-scale field tests (Berger <i>et al.</i> 2011; Wendeler 2008) and proposed a stepwise load model to estimate the impact forces on the flexible barrier during the interaction with a debris flow. The hydro-dynamic approach and the hydro-static approach were applied in that model. The hydro-dynamic approach with the dynamic coefficient $c_w=2.0$ for granular flows suggested in that literature can accurately evaluate the impact forces on the flexible ring net measured in our large-scale tests. This literature also assumed that the impact loading from a debris flow applied on a flexible barrier is evenly distributed over the barrier. This assumption was proved by back-calculation using the data from field tests, which supports the assumption made in our draft paper that the impact pressure in the measured area can reflect the impact loading on the impact area of the flexible ring net (see Page 14 Lines 332-335).  To improve the quality of the draft paper: nhess-2018-131, the suggested literature has been comprehensively reviewed and appropriately cited. The revised and added

		<p>contents are marked as blue underlined fonts in the revised draft:</p> <ol style="list-style-type: none"> <li>1) Page 3-4 (Lines 77-82).</li> <li>2) Page 4-5 (Lines 102-104).</li> <li>3) Review of the literature in Page 6 (Lines 132-144).</li> <li>4) Page 6 (Lines 147-148).</li> <li>5) Pages 11-12 (Lines 272-277).</li> <li>6) We used the measured impact forces of the dry granular flow to verify the hydro-dynamic approaches with two dynamic coefficients proposed by Wendeler (2008): <math>c_w=2.0</math> for granular flows and <math>c_w=0.7</math> for muddy debris flows. See Pages 17-18 (Lines 410-412), Page 18 (Lines 417-428) and Table 3 (Page 27).</li> <li>7) Add the suggested literature into the reference list: Page 24 (Lines 585-587).</li> </ol>
3	<p>I have one final question: did you measure the "pile-up" density behind the net? In the table you report the bulk density (1600 kg/m<sup>3</sup>), but I was wondering if you have any idea of the compacted density behind the net.</p>	<p>Reply: Thanks for raising this valuable question and the insightful suggestion. We did not measure the compacted density behind the net in the conducted tests. But we believe that both the flowing density before the impact and the density during the deposition after impact shall be measured in the future tests with the assistance of laser devices and force plates. We had measured only the loose dry bulk density of the aggregate material according to ASTM C29/C29M-91a (ASTM 2009) before we conducted the dry granular flow impact tests. The bulk density of the dry aggregate with the value of 1600 kg/m<sup>3</sup> fits well with the testing results in the literatures (Rücknagel <i>et al.</i> 2007, Raj <i>et al.</i> 2014, Yahia and Kabagire 2014). To avoid the confusion, we have clarified the determination of the dry bulk density in Page 9 (Lines 220-221) and Page 22 (Lines 511-512) for adding the reference.</p> <p>When a dry granular flow is stopped by a flexible barrier, the deposited aggregate is compacted by the oncoming debris front, and the bulk density of the aggregate deposited behind the barrier increases correspondingly. Therefore, the density used in the hydro-static model should be different from the density used in the hydro-dynamic model. However, Wendeler <i>et al.</i> (2018) used the same debris density in the hydro-static model as that in the</p>

		hydro-dynamic model, because the magnitude of the static pressure could be reduced due to the stability increase of the deposited debris compared to the flowing debris. Undoubtedly, it is highly worthy to quantify the density and the stability change before and after the impact and the deposition process in the future studies.
--	--	--

### References:

- ASTM, C. Standard test method for bulk density (“unit weight”) and voids in aggregate, 2009.
- Berger, C., McArdell, B.W., Schlunegger, F. Direct measurement of channel erosion by debrisflows, Illgraben, Switzerland. *J. Geophys. Res.* 116, F01002, doi: 10.1029/2010JF001722: 18 p, 2011.
- Raj, N., Patil, S.G. and Bhattacharjee, B. Concrete mix design by packing density method. *IOSR J. Mech. Civ. Eng.* 11(2), pp.34-46, 2014.
- Rücknagel, J., Hofmann, B., Paul, R., Christen, O. and Hülsbergen, K.J. Estimating precompression stress of structured soils on the basis of aggregate density and dry bulk density. *Soil and Tillage Research*, 92(1-2), pp.213-220, 2007.
- Wendeler, C. S. I. Murgangrückhalt in Wildbächen. Grundlagen zu Planung und Berechnung von flexiblen Barrieren. ETH, 2008.
- Wendeler, C., Volkwein, A., McArdell, B.W. and Bartelt, P. Load model for designing flexible steel barriers for debris flow mitigation. *Canadian Geotechnical Journal*, (ja), 2018.
- Wendeler, C., and Volkwein, A. Laboratory tests for the optimization of mesh size for flexible debris-flow barriers. *Natural Hazards and Earth System Sciences*, 15(12), 2015.
- Yahia, A. and Kabagire, K.D. New approach to proportion pervious concrete. *Construction and Building Materials*, 62, pp.38-46, 2014.

**“Large Scale Physical Modelling Study of a Flexible Barrier under the Impact of Granular Flows” (nhess-2018-131)**

**Reply to Review Comments from the Referees**

**by Dao-yuan TAN and Co-Authors**

The authors wish to thank the referees for their insightful and constructive comments on the manuscript and advice to us for improving the quality of the draft paper. The authors have taken full consideration of all those comments and made clarification and corrections in following tables:

**Replies to Referee 1’s comments:**

No.	Referee 1’s comments	Reply
1	How did the authors define the word large-scale in their experiments?	Reply: This is a very good question. The definition of large-scale in our tests (PolyU model) is based on the definition of the large-scale physical model built by USGS (Iverson <i>et al.</i> 2010; Iverson 2015). The physical model built in PolyU site has similar dimensional parameters to the USGS debris-flow flume. Specifically, the capacity of testing material is 5 m <sup>3</sup> in PolyU model compared to 10 m <sup>3</sup> in USGS flume, and the width of the flume is 1.5 m in PolyU model compared to 2 m in USGS flume. Even though the length of the flume in PolyU model is much shorter than the length of USGS flume (7 m compared to 95 m), the flume in PolyU model is sufficient to generate debris flows with dynamic parameters similar to real cases. In the trial tests, the generated watery flood can reach a velocity higher than 8 m/s during the flowing down. In the generated granular flow, the flow velocity (5 m/s), the measured impact force (10.96 kN) and the deposition mechanism are similar to the parameters of debris flows in literatures (Bugnion and Wendeler 2010; Arattano and Marchi 2005). Thus, we regard Polyu model as a large-scale physical model. Related explanation has been added into the manuscript in Page 8 (Lines 179-189).

2	In lines195-197, how did the authors define the deposition height of the granular flow, and the maximum horizontal deformation of the flexible barrier? It is better to show them in the scratch.	Reply: Thanks for the valuable comment, we have added the definitions of the deposition height and the maximum horizontal deformation of the flexible barrier in Page 10, Lines 244-247 and Fig.5 in Page 34.
3	What are the unique advantages of the experiments performed in this paper compared to the other researches, as the authors stated that an improved large-scale physical modelling facility for debris flow research has been conducted?	Reply: The description of the improved large-scale physical model is to emphasize that the physical modelling device is improved by a fast door opening system (see Page 7, Line 168). With the fast door opening system, the door can be flipped up quickly (shorter than 0.5 s) after triggering to minimize the interference from the door and increase the uniformity of the generated granular flows. Besides, a new method is utilized to directly measure the impact forces on the flexible ring net (Section 4.1), which is another improvement of the experiment device in this paper.
4	How many Test1 and Test2 experiments were performed by the authors? It would be great if the authors can comment how the experimental results vary between different rounds of experiments.	Reply: Thanks for the comments, and we only did once for each test. We will consider conducting more tests in the future by changing parameters of granular flows and flexible barriers. However, it is difficult to perform more tests within a short period due to the long preparation time of each test.
5	In Table 1, how did the authors determine the internal friction angle and the interface friction angle for granular flows?	Reply: The internal friction angle of the aggregate, which is regarded having the same value with the angle of repose (Hutter and Koch 1991), is measured by the pouring test introduced by Miura <i>et al.</i> (1997) and Zhou <i>et al.</i> (2014). The interface friction angle is determined by the tilting plane method introduced by Hutter and Koch (1991) and Zhou <i>et al.</i> (2014). The above description has been added in the manuscript (Page 9, Lines 221-225).
6	In the 4th column of Table 3, the unit kN should not be italic.	Reply: Noted with thanks, we have corrected it in the manuscript.

## References

- Arattano, M. and Marchi, L. Measurements of debris flow velocity through cross-correlation of instrumentation data. *Natural Hazards and Earth System Science*, 5(1), 137-142, 2005.
- Bugnion, L. and Wendeler, C. Shallow landslide full-scale experiments in combination with testing of a flexible barrier. *WIT Transactions on Engineering Sciences*, 67, 161-173, 2010.
- Hutter, K. and Koch, T. Motion of a granular avalanche in an exponentially curved chute: experiments and theoretical predictions. *Phil. Trans. R. Soc. Lond. A*, 334(1633), 93-138, 1991.
- Iverson, R.M. Scaling and design of landslide and debris-flow experiments. *Geomorphology*, 244, 9-20, 2015.
- Iverson, R.M., Logan, M., LaHusen, R.G. and Berti, M. The perfect debris flow? Aggregated results from 28 large-scale experiments. *Journal of Geophysical Research: Earth Surface*, 115(F3), 2010.
- Miura, K., Maeda, K. and Toki, S. Method of measurement for the angle of repose of sands. *Soils and Foundations*, 37(2), 89-96, 1997.
- Zhou, G.G., Ng, C.W. and Sun, Q.C. A new theoretical method for analyzing confined dry granular flows. *Landslides*, 11(3), 369-384, 2014.

## Replies to Referee 2's comments:

No.	Referee 2's comments	Reply
1	Page 5: value of 2.0 proposed by Wendeler in 2008: PHD Thesis ETH No 17916	Reply: Thanks for your correction, we have corrected this citation error in Page 5 (Line 122-124) and Table 3.
2	Page 7: velocity of the flow only calculated by the high speed videos? Very roughly, no laser devices in front of the barrier?	Reply: Thanks for your valuable suggestions. We agree that more measuring devices will increase the accuracy of measurement, and we will consider adding more measuring devices such as laser devices to better determine the flow velocity and depth. However, in this study, the velocity of the granular flow was merely measured from continuous photographs taken by the side-view high-speed camera. To increase the accuracy of the measurement, two actions were taken: firstly, we set the location and the shooting angle of the side-view high speed camera very carefully to make sure that the camera was perpendicular to the transparent side wall of the flume; secondly, the impact velocity of the granular flow was determined from the average value of the velocities of 5 particles measured from 5 continuous photographs with the assistance of the reference lines attached to the flume. Related explanation of the measurement has been added into the manuscript in Page 9 (Lines 209-216).
3	Page 8: 5 m/s can be for granular flow in the correct range but I am wondering about bulk density given with 1600 kg/m <sup>3</sup> fitting not in the range of granular flow which normally have around 2000 kg/m <sup>3</sup> (page 22) and more.	Reply: We agree that the typical bulk density of granular debris flows is around 2000 kg/m <sup>3</sup> , but the testing material in our study is dry aggregate with a large percentage of void space and a lower bulk density. We measured the loose dry bulk density of the aggregate material according to ASTM C29/C29M-91a (ASTM 2009) before we conducted the dry granular flow impact tests. The bulk density of the dry aggregate with the value of 1600 kg/m <sup>3</sup> fits well with the testing results in the literatures (Rücknagel <i>et al.</i> 2007, Raj <i>et al.</i> 2014, Yahia and Kabagire 2014). To avoid the confusion, we have clarified the determination of the dry bulk density in Page 9 (Lines 220-221) and Page 22 (Lines 511-512) for adding the reference. In the future, we will conduct more tests using a mixture of aggregate and

		saturated slurry, which is predicted to have higher densities much closer to the common value of 2000 kg/m <sup>3</sup> .
4	Page 10: Second surge not realistic for reality, because the material was already drained. How long was the time in between the two surges? In a real debris flow it happens all together very quickly, there is no time of drainage	Reply: The time interval between two tests is around 2 weeks, because we need at least 2 weeks to prepare a test. We agree that the drainage of the debris deposition should be considered in the study of multiple debris flows, and we plan to do related tests in the future. In our study, the research subject is dry granular flow. Thus, drainage should not be a problem. Many thanks for your suggestions, and we will be more careful in conducting impact tests with saturated debris flows in the future.
5	Page 12, line 279 it is Figure 12 instead of Figure 10.	Reply: Thanks for your correction, we have corrected it in the manuscript.
6	Page 16: Two tests is nothing for research background and statistic interpretation. You need more tests to interpret the results correctly. Second test is not useful because front was stopped, no dynamic impact onto the barrier.	Reply: Thanks for your suggestions. We strongly agree that more tests can enhance the reliability of the quantitative conclusions drawn in this study, but one successful large-scale physical modelling test can clearly investigate the impact mechanisms of a granular flow with poor fluidity on a flexible barrier. We also believe that the verification of simple approaches using the impact forces on different components is also valuable to the future research and the design of debris flow flexible barrier. Besides, the verification results fit well with the conclusions drawn in the literatures (Wendeler 2008, Wendeler <i>et al.</i> 2018). Even the granular flow in Test 2 was stopped before it can reach the flexible barrier due to the poor fluidity of dry granular flows, it still can provide valuable data and reference to the study of the motion and the deposition of the second surge in a multiple debris flow event.
7	Page 17: explain and discuss the results together with table 3 page 24. It must be more clearly explained where the results come from.	Reply: Thanks for the valuable suggestions. With the conclusions drawn from the large-scale tests presented in this draft paper, it can be preliminarily concluded that the impact force on the flexible ring net and on the supporting structures are different due to the large deformation of the flexible ring net, thus the loadings on them should be estimated



		<p>separately using different simple approaches or an appropriate value of Loading Reduction Rate (LRR). Thus, the design of a flexible barrier for debris flow mitigation can be optimized by dimensioning and designing the flexible ring net and the supporting structures individually with appropriate design loadings, which provides a safer and more economical design method.</p> <p>A specified explanation has been added into the manuscript (Lines 477 to 485).</p>
8	<p>Page 17: I still believe that <math>c=2.0</math> is representing the granular impact on flexible barriers but we need more test results.</p>	<p>Reply: We agree. The dynamic coefficient of 2.0 has been verified by the measured impact force on the flexible ring net in the large-scale test (see Table 3). This approach can accurately estimate the impact of a granular flow on a flexible barrier. More tests are under consideration to further verify simple approaches using different debris materials such as muddy debris flows.</p>

**References:**

- ASTM, C. Standard test method for bulk density (“unit weight”) and voids in aggregate, 2009.
- Raj, N., Patil, S.G. and Bhattacharjee, B. Concrete mix design by packing density method. *IOSR J. Mech. Civ. Eng.*, 11(2), pp.34-46, 2014.
- Rücknagel, J., Hofmann, B., Paul, R., Christen, O. and Hülsbergen, K.J. Estimating precompression stress of structured soils on the basis of aggregate density and dry bulk density. *Soil and Tillage Research*, 92(1-2), pp.213-220, 2007.
- Wendeler, C. S. I. Murgangrückhalt in Wildbächen. Grundlagen zu Planung und Berechnung von flexiblen Barrieren. ETH, 2008.
- Wendeler, C., Volkwein, A., McArdell, B.W. and Bartelt, P. Load model for designing flexible steel barriers for debris flow mitigation. *Canadian Geotechnical Journal*, (ja), 2018.
- Yahia, A. and Kabagire, K.D. New approach to proportion pervious concrete. *Construction and Building Materials*, 62, pp.38-46, 2014.

1 **Large Scale Physical Modelling Study of a Flexible Barrier under the**  
2 **Impact of Granular Flows**

3  
4 by

5 **Dao-Yuan TAN**

6 Department of Civil and Environmental Engineering  
7 The Hong Kong Polytechnic University, Hung Hom, Kowloon, Hong Kong, China  
8 Email: t.daoyuan@connect.polyu.hk  
9

10 **Jian-Hua YIN** (Chair Professor and Corresponding Author)

11 Department of Civil and Environmental Engineering  
12 The Hong Kong Polytechnic University, Hung Hom, Kowloon, Hong Kong, China  
13 Tel: (852) 2766-6065, Fax: (852) 2334-6389, Email: cejhyin@polyu.edu.hk  
14

15 **Wei-Qiang FENG**

16 Department of Civil and Environmental Engineering,  
17 The Hong Kong Polytechnic University, Hung Hom, Kowloon, Hong Kong, China  
18 Email: fengweiqiang2015@gmail.com  
19

20 **Jie-Qiong QIN**

21 Department of Civil and Environmental Engineering  
22 The Hong Kong Polytechnic University, Hung Hom, Kowloon, Hong Kong, China  
23 Email: jieqiong.qin@connect.polyu.hk  
24

25 And

26 **Zhuo-Hui ZHU**

27 Department of Civil and Environmental Engineering  
28 The Hong Kong Polytechnic University, Hung Hom, Kowloon, Hong Kong, China  
29 Email: zhuo-hui.zhu@connect.polyu.hk  
30  
31

32  
33  
34 Manuscript submitted to *Natural Hazards and Earth System Sciences* for possible  
35 publication as a Technical Paper  
36  
37

38 September 2018  
39

40 **Abstract:**

41 Flexible barriers are being increasingly applied to mitigate the danger of debris flows.  
42 However, how barriers can be better designed to withstand the impact loads of debris  
43 flows is still an open question in natural hazard engineering. Here we report an  
44 improved large-scale physical modelling device and the results of two consecutive  
45 large-scale granular flow tests using this device to study how flexible barriers react  
46 under the impact of granular flows. In the study, the impact force directly on the flexible  
47 barrier and the impact force transferred to the supporting structures are measured,  
48 calculated and compared. Based on the comparison, the impact loading attenuated by  
49 the flexible barrier is quantified. The hydro-dynamic approaches with different  
50 dynamic coefficients and the hydro-static approach are validated using the measured  
51 impact forces.

52 **KEYWORDS:** Large-scale tests; granular flow; flexible barrier; impact loading

53

54 **1. Introduction**

55 Debris flows, as one of the most disastrous natural geohazards, have caused destructive  
56 damage to human lives and their habitations in many countries such as USA, Japan,  
57 and China (Takahashi 2014; Hungr 1995; Ishikawa *et al.* 2008; Su *et al.* 2017). In a  
58 mountainous area where a large amount of loose sediment is present, multiple debris  
59 flows can occur under intensive heavy rains (Xu *et al.* 2012; Yagi *et al.* 2009; Chen *et*  
60 *al.* 2017). Protective systems such as concrete check dams are usually installed in areas  
61 threatened by debris flows to prevent the damage (Santi *et al.* 2011). Nowadays,  
62 researchers have found that flexible barriers, which were firstly used in rockfall  
63 prevention, are effective to trap debris flows (Canelli *et al.* 2012; Wendeler *et al.* 2007;  
64 Cui *et al.* 2015; Hu *et al.* 2006; Kwan *et al.* 2014). Compared to conventional rigid  
65 concrete check dams, flexible barriers have a few obvious advantages: economical,  
66 efficient in impact energy absorption, easy to be installed and adaptable to various  
67 terrains (Ashwood and Hungr 2016; Wendeler and Volkwein 2015).

68

69 Physical modelling has been widely used in geotechnical engineering research because  
70 of its excellent controllability in testing conditions and good reliability of testing results  
71 (Paik *et al.* 2012; Wendeler *et al.* 2006; Bugnion *et al.* 2012; DeNatale *et al.* 1999).

72 Scaling is a key parameter in experiment design for studying debris flows because it  
73 can affect the interaction between particles in a granular flow. In miniaturized debris  
74 flows generated in small-scale tests, the effects of viscous shear resistance, friction, and  
75 cohesion are over-represented, whereas the effects of excess pore-fluid pressure, which  
76 are generated by debris dilation or contraction, are under-represented (Iverson 2015).

77 [With appropriate dimensional analysis, laboratory tests can be used to qualitatively](#)  
78 [study behavior of the interaction between a debris flow and a flexible barrier \(Wendeler](#)

79 [and Volkwein 2015, Wendeler \*et al.\* 2018, Song \*et al.\* 2017\)](#). However, the dynamic  
80 [behavior of different barrier components of a prototype flexible barrier and the stiffness](#)  
81 [of the flexible ring nets applied in the field are difficult to be reliably replicated in](#)  
82 [miniaturized physical models \(Wendeler \*et al.\* 2018\)](#). Considering the scale effects,  
83 some researchers use large-scale physical models or field-scale experimental sites to  
84 study debris flows (DeNatale *et al.* 1999; Wendeler 2008; Paik *et al.* 2012; Bugnion *et*  
85 *al.* 2012; Iverson 2015). WSL (2010) conducted a series of full-scale tests to study the  
86 interaction between multiple debris flows and a prototype flexible barrier. Large-scale  
87 physical modelling tests are also selected by the authors to investigate the interaction  
88 between a flexible barrier and dry granular flows.

89

90 A typical flexible barrier usually consists of two main components: a flexible ring net  
91 and supporting structures (supporting posts stretching the flexible barrier, strand cables  
92 and foundations supporting the posts). The impact loading from a debris flow is firstly  
93 attenuated by the flexible ring net with large deformation, then transfers to the cross-  
94 tension cables, which form the outline frame and stretch the ring net, and finally to the  
95 posts and the supporting cables. Generally, energy dissipating elements are installed on  
96 the supporting cables to reduce load peaks transferred to the foundations (Volkwein  
97 2014; Wendeler *et al.* 2018). In this study, energy dissipating elements are replaced by  
98 large capacity tension link transducers to accurately measure the impact loading  
99 transferred to the supporting structures.

100

101 Impact loading estimation is key to the design of a flexible barrier for debris flow  
102 mitigation (Volkwein *et al.* 2011). [Wendeler \*et al.\* \(2018\) concluded that the static](#)  
103 [pressure on the flexible barrier is dominant and gradually increases with time during](#)

104 [the impact process based on the observations of field tests](#). Simple approaches are  
105 commonly used by designers in impact loading estimation because they require only a  
106 few parameters in the calculation. There are two widely accepted simple approaches:  
107 the hydro-dynamic approach and the hydro-static approach. The hydro-dynamic  
108 approach is based on momentum conservation. In this approach, the impact period is  
109 taking as an ideal flow with a uniform velocity impacting the barrier and deviating  
110 along the vertical direction. The impact loading is calculated from the momentum  
111 change of the decelerated debris flow during the impact (Hungr *et al.* 1984; Armanini  
112 1997). The hydro-static approach, on the other hand, is calculated from the earth  
113 pressure of deposited debris (Rankine 1857). Both approaches adopt empirical  
114 coefficients to reach a good accuracy in predicting real cases.

115

116 The estimation of impact force with the hydro-dynamic approach (Hungr *et al.* 1984)  
117 is expressed as follows:

$$118 \quad F_{calculated} = \alpha \rho_{bulk} v_0^2 h w \quad (1)$$

119 where  $\rho_{bulk}$  is the bulk density of a debris flow,  $v_0$  is the velocity of the debris flow,  $h$  is  
120 the height of the debris flow,  $w$  is the width of the debris flow, which is normally  
121 represented by the width of the flowing channel, and  $\alpha$  is the dynamic coefficient.  
122 Hungr *et al.* (1984) proposed a value of 1.5. Wendeler (2008) suggested a value of 0.7  
123 for mud flows and 2.0 for granular flows considering the flexibility and permeability  
124 of flexible barriers. Canelli et al (2012) proposed a range of values from 1.5 to 5.

125

126 The hydro-static approach (Lichtenhahn 1973; Armanini 1997) is given as follows:

$$127 \quad F_{calculated} = \kappa \rho_{bulk} g h_{deposit}^2 w \quad (2)$$

128 where  $\kappa$  is the static coefficient, which is suggested as 1.0 in the calculation (Kwan and

129 Cheung 2012; Wendeler *et al.* 2018).  $g$  is gravitational acceleration, and  $h_{deposit}$  is the  
130 deposition height of the debris flow.

131

132 Wendeler *et al.* (2018) proposed a stepwise load model to describe the impact pressures  
133 on the flexible barrier during the impact process. In this model, the hydro-dynamic  
134 approach with the dynamic coefficient of 0.7 for mud flows and 2.0 for granular flows  
135 and the hydro-static approach with the static coefficient of 1.0 are used to calculate the  
136 dynamic impact loading from the moving debris flow and the earth pressure from the  
137 static debris deposition, respectively. The whole impact process was divided into three  
138 impact stages: the initial impact, the filling stage and the overflow stage. In the initial  
139 impact stage, there was only dynamic impact loading on the flexible barrier. In the  
140 filling stage, the loading combination on the flexible barrier contained both the dynamic  
141 impact loading and the static earth pressure. In the overflow stage, only the static  
142 loading from the deposited debris and the overflowed debris flow exerted on the flexible  
143 barrier. This method was verified by the tensile forces on the supporting cables of a  
144 flexible barrier in the field tests.

145

146 However, the interaction between a flexible barrier and multiple granular flows has not  
147 been fully understood. Values of the suggested coefficients used in the hydro-dynamic  
148 and hydro-static approaches need to be further verified. The efficiency of loading  
149 reduction by flexible barriers has not been accurately quantified. Therefore, further  
150 research on the impacts of debris flows on a flexible barrier is urgently required.

151

152 This paper aims to study the motions of multiple granular flows and the performance  
153 of a flexible barrier under the impact of granular flows with large-scale physical

154 modelling tests. The data from well-arranged transducers and high-speed cameras in  
155 the debris flow impact tests are presented and analyzed in this paper. The motions of  
156 two consecutive granular flows are described in detail. The impact forces on the flexible  
157 ring net and the supporting structures of the flexible barrier are measured respectively.  
158 Using the measured results, the contribution of flexibility to impact loading reduction  
159 is quantified, and simple approaches with different coefficients for impact force  
160 estimation are verified.

161

## 162 **2. Experiment setup and instrumentation**

### 163 *2.1 Description of the experiment apparatus*

164 A testing device is built in the Road Research Lab of the Hong Kong Polytechnic  
165 University with a length of 9.5 m, a height of 8.3 m and a width of 2 m. The view of  
166 the experiment setup is plotted in Fig.1. This facility can be divided into 4 main  
167 components: (i) a reservoir with the capacity of 5 m<sup>3</sup> at the top of the device, (ii) a novel  
168 quick flip-up door opening system at the front vent of the reservoir, (iii) a prototype  
169 flexible barrier with supporting posts and cables, and (iv) a flume linking the reservoir  
170 and the flexible barrier. The prototype flexible barrier with a width of 2.48 m is made  
171 up of steel rings with a diameter of 300 mm (No. ROCCO 7/3/300, Geobruigg), which  
172 are commonly used in rockfall mitigation in European and Hong Kong. This ring net is  
173 covered by a flexible secondary net with the mesh size of 50mm to provide a high  
174 trapping rate for the granular flows. Two parallel posts that can rotate in the plane of  
175 impact are installed to stretch and support the ring net, and each post is supported by  
176 two inclined strand cables. The flume has a length of 7 m, an inner width of 1.5 m and  
177 an inclination angle of 35 °. Side walls of the flume are made up of tempered glass to  
178 provide a clear observation to the generated granular flows and their interactions with



179 the flexible barrier. Based on the parameters of the large-scale physical model built by  
180 USGS (Iverson *et al.* 2010; Iverson 2015), the physical model built in the Hong Kong  
181 Polytechnic University (PolyU model) can be regarded as a large-scale physical model  
182 because it has similar dimensional parameters with respect to the USGS debris-flow  
183 flume. Specifically, the capacity of testing material is 5 m<sup>3</sup> in PolyU model compared  
184 to 10 m<sup>3</sup> in USGS flume, and the width of the flume is 1.5 m in PolyU model compared  
185 to 2 m in USGS flume. Even though the length of the flume in PolyU model is much  
186 shorter than the length of USGS flume (7 m compared to 95 m), the flume in PolyU  
187 model is sufficient to generate debris flows with dynamic parameters and impact energy  
188 similar to real cases. In the trial tests, the generated watery flood can reach a velocity  
189 higher than 8 m/s during the flowing down.

190

## 191 **2.2 Instrumentation**

192 To monitor the performance of a flexible barrier under the impact of granular flows,  
193 this device is instrumented with a well-arranged high-frequency measurement system.  
194 Two types of transducers are installed on the flexible protection system: mini tension  
195 link transducers and high capacity tension link transducers. The mini tension link  
196 transducers were calibrated in the soil laboratory with a maximum loading of 20 kN.  
197 The calibration is plotted in Fig.2. Those transducers are installed on the flexible ring  
198 net to measure the impact force on the flexible ring net directly. Specifically, the central  
199 area of the flexible ring net, which consists of 5 connected rings, is separated from the  
200 main net and reconnected to the neighboring rings by 10 mini tension link transducers.  
201 Fig.3 presents the measured central area and the arrangement of all the mini tension  
202 link transducers on the flexible ring net. The high capacity tension link transducers with

203 a certified capacity of 50 kN are installed on the supporting cables of the posts (see  
204 Fig.1 (b)). A data-logger with the capability of sampling 48 transducers at 1000 Hz  
205 simultaneously is used to collect the data of all transducers. Two high-speed cameras  
206 capable of capturing a resolution of  $1024 \times 768$  pixels at a sampling rate of 1000 frames  
207 per second are used to capture the motions of the granular flows and the deformation  
208 of the flexible barrier under impact. One high-speed camera is located at the right side  
209 of the barrier, and the other one is set in front of the barrier. The impact velocity of the  
210 debris flow was measured from continuous photographs taken by the side-view high-  
211 speed camera. To increase the accuracy of the measurement, two measures were taken:  
212 firstly, we set the location and the shooting angle of the side-view high speed camera  
213 very carefully to make sure that the camera was perpendicular to the transparent side  
214 wall of the flume; secondly, the velocity was determined from the average velocities of  
215 5 individual particles measured from 5 continuous photographs before the impact with  
216 the assistance of the reference lines attached to the flume.

217

### 218 ***2.3 Experiment material and procedures***

219 The sample of material used in the tests is plotted in Fig.4, and their properties are listed  
220 in Table 1. The bulk density of the aggregate is determined from the loose dry bulk  
221 density according to ASTM C29/C29M-91a (ASTM 2009) before the tests. The internal  
222 friction angle of the aggregate, which is regarded having the same value with the angle  
223 of repose, is measured by the pouring tests introduced by Miura *et al.* (1997) and Zhou  
224 *et al.* (2014). The interface friction angle is determined by the tilting plane method  
225 introduced by Hutter and Koch (1991) and Zhou *et al.* (2014). Two consecutive tests,  
226 named Test 1 and Test 2 were conducted using the same granular material. In test 1, the  
227 granular flow travelled via the flume and impacted an empty flexible barrier. While in

228 Test 2, the granular flow moved on the upper surface of the deposition in Test 1 to  
229 simulate the second surge in multiple flows. The progress of each test is described as  
230 follows. At the beginning of the test, the door was flipped up in less than 0.5 s with the  
231 help of a fast door opening system to generate a uniform granular flow. The datalogger  
232 started to obtain data several seconds before the triggering of the granular flow to obtain  
233 initial values of all the transducers. Simultaneously, the high-speed cameras started to  
234 capture the motion of the granular flow and its interaction with the flexible barrier  
235 during the impact.

236

### 237 **3. Test results**

#### 238 ***3.1 Motion and impact of granular flow in Test 1***

239 In test 1, the initial time of the impact has been readjusted to 0 s in all plotted data and  
240 selected video frames, and the negative value of time represents the moment before the  
241 interaction. By tracking the motion of the granular flow with high-speed cameras, the  
242 speed of the granular flow was 5 m/s, which was relatively low compared with the  
243 measured velocities from 2 m/s to 12 m/s in literatures (Arattano and Marchi 2005;  
244 Prochaska *et al.* 2008; Berti *et al.* 1999). The deposition height of the granular flow and  
245 the maximum horizontal deformation of the flexible barrier at different times are  
246 measured from the profiles of the granular flow in photographs taken by the side-view  
247 high-speed camera during the impact period (see Fig.5). It can be observed from Fig.5  
248 that the front portion of the granular flow shot up, impacted the barrier directly and  
249 deposited as a wedge-shaped dead zone at the bottom of the flexible barrier from 0 s to  
250 1.0 s. The following granular flow climbed on the top surface of the previous stationary  
251 deposition, impacted the flexible barrier, and deposited behind the barrier layer by layer.

252 After 1.0 s, the following granular front deposited behind the deposition wedge. It is  
253 worth noting that the tensile force on the net keeps increasing even the deposition height  
254 of the granular flow reach the maximum value. This phenomenon indicates that the  
255 granular flow can continuously exert impact pressure on the flexible barrier via the  
256 deposition wedge. The measured deposition height, the maximum horizontal  
257 deformation and the tensile force history of Transducer 1 change with time are plotted  
258 in Fig.6. It can be seen that the deposition height of the trapped aggregate rises almost  
259 linearly with time and reaches 0.55 m at the time of 1.0 s, and the horizontal  
260 deformation of the barrier increases from an initial value of 0.262 m to 0.481 m at the  
261 time of 1.0 s.

262

### 263 ***3.2 Impact loading analysis in Test 1***

264 Tensile forces recorded by the mini tension link transducers between rings are plotted  
265 in Fig.7. Signals of the transducers have some noises due to the intensive impacts from  
266 thousands of particles during the impact period. Thus, trend lines are added into those  
267 figures to clarify the changes of tensile forces. A gradual rise of static load and two  
268 dynamic impact peaks are observed in the signals of most transducers. The first impact  
269 peak occurred at the beginning of the impact, and the second impact peak appeared at  
270 the end of the impact. These two peaks are much smaller than the accumulated static  
271 load. It is indicated that the dynamic load and the static load co-existed in the impact  
272 process, and the static load was dominant. [The loading situations of the flexible barrier  
273 in our study fits well with the observations of the field tests by Wendeler \*et al.\* \(2018\)  
274 that the impact loadings on the supporting ropes increase gradually over time during  
275 the impact process. Since the dynamic loading due to the oncoming debris fronts is](#)

276 [nearly constant, they concluded that the increase of the impact loading mainly attributes](#)  
277 [to the incremented debris deposition.](#) Besides, transducers connected to the bottom  
278 cross-tension cable (Transducer 7 and Transducer 8) show negative values, which  
279 indicates that they were compressed in the impact process. Fig.8 presents typical frames  
280 recorded by the side-view camera and the front-view camera combined with the signal  
281 from Transducer 1. From this figure, it can be indicated that the first dynamic impact  
282 peak came from the direct impact of the first debris front on the flexible barrier, and the  
283 gradual increase of the static load was caused by the deposition of the aggregate. With  
284 the growth of the deposition zone, the impact loading of the following granular flow  
285 was finally fully resisted by the deposition cushion. Afterwards, only static earth  
286 pressure of the deposition acted on the flexible barrier.

287

### 288 ***3.3 Motion of granular flow in Test 2***

289 The second granular flow was triggered after Test 1 to simulate the second flow in a  
290 multiple debris flow event. In Test 2, the granular flow travelled on the top surface of  
291 the deposition in Test 1 and came to rest without reaching the net. The motion of the  
292 granular flow in Test 2 is plotted in Fig.9. In that figure, the initiated time of the granular  
293 flow is readjusted to 0 s. It can be found that the granular flow had a thick front when  
294 it was firstly triggered, then the thickness kept decreasing during movement. Based on  
295 the recording of the side-view camera, the side-view of depositions in the two tests and  
296 the velocity change of the granular flow with the flowing distance in Test 2 are plotted  
297 in Fig.10. The thickness and velocity of the front reduced dramatically with the increase  
298 of the moving distance and finally stopped at 0.7 m before the flexible barrier.  
299 Correspondingly, no impact force and deformation increment of the flexible barrier

300 were recorded by the transducers and the high-speed cameras. The reason for the flow  
301 stopping before the flexible barrier is the large basal friction of the rough interface  
302 between the moving granular flow and the deposition and the low fluidity of the dry  
303 granular flow. The multi-flow tests show that the impact from the latter arrived debris  
304 flows can be attenuated or eliminated by the resistance from the deposition of the  
305 previous debris flow in a multiple debris flow event.

306

## 307 **4. Data analysis**

### 308 *4.1 Direct measurement of the impact force on the flexible barrier*

309 As mentioned above, the central area is separated from the main ring net and  
310 reconnected to neighboring net rings by mini tension link transducers. Two assumptions  
311 are made to simplify the measurement of the impact loading on a flexible ring net. The  
312 deformation of the ring net is assumed similar to a membrane, and the deformation in  
313 the measured area is assumed cone symmetric. Based on the assumptions, the loading  
314 situation in the cross-section of the measured area which contains Transducer  $i$  and  
315 Transducer  $i+1$  is analyzed and shown in Fig.11. Thus, the impact force on the cross-  
316 section can be calculated with the following equation:

$$317 \quad F_{impact,i,i+1} = F_{tensile,i} \cdot \cos \frac{\theta}{2} + F_{tensile,i+1} \cdot \cos \frac{\theta}{2} \quad (3)$$

318 where  $F_{tensile,i}$  and  $F_{tensile,i+1}$  are the maximum tensile forces on Transducer  $i$  and  
319 Transducer  $i+1$  installed in the measured area,  $\theta$  is the included angle between the  
320 opposite transducers,  $F_{impact,i,i+1}$  is the calculated impact force on this cross-section.  
321 Since the deformation in the measured area is assumed cone symmetric,  $\theta$  is a constant  
322 in all cross-sections formed by two opposite transducers. Thus, for the measured area

323 with  $n$  transducers, the maximum impact force,  $F_{measured}$ , can be calculated with the  
324 following equation:

$$325 \quad F_{measured} = \cos \frac{\theta}{2} \cdot \sum_{i=1}^{i=n} F_{tensile,i} \quad (4)$$

326 In our study, the maximum tensile forces on all transducers are measured and plotted  
327 in Fig.12, and  $\theta$  can be measured from the photograph taken at the moment of the largest  
328 deformation as shown in Fig.13.

329

330 The impact pressure from the granular flow is assumed to be uniformly distributed in  
331 the cross-section area of the flume width multiplied by the height of the debris  
332 deposition, which covers the measured central area. [The uniformly distributed impact  
333 loading on the flexible ring net has been proved by back-calculation using the tensile  
334 forces and deformations of the horizontal supporting cables of the flexible barrier in  
335 field tests \(Wendeler \*et al.\* 2018\).](#) Combined with Eq. 4, the following equation is given  
336 to calculate the distributed impact loading on a flexible ring net:

$$337 \quad F_{impact} = F_{measured} \cdot \frac{A_{impact}}{A_{measured}} = \cos \frac{\theta}{2} \cdot \sum_{i=1}^{i=n} F_{tensile,i} \cdot \frac{A_{impact}}{A_{measured}} \quad (5)$$

338 where  $A_{impact}$  and  $A_{measured}$  represent the actual impact cross-section area and the  
339 measured central area in the test as shown in Fig.12. All the parameters and calculated  
340 results are listed in Table 2.

341

#### 342 **4.2 Calculation of Loading Reduction Rate (LRR)**

343 The flexible ring net is supported by two posts that can rotate in the plane of the flow  
344 direction, and each post is supported by two inclined steel strand cables. Therefore, the  
345 impact force transferred from the flexible barrier to the supporting posts can be

346 calculated from the tensile forces carried by the supporting cables in the direction of  
 347 impact. Based on the symmetrical arrangement of the cables and the posts with respect  
 348 to the flexible barrier, as plotted in Fig.14 (a), the loading situations of the posts and  
 349 the supporting cables located on both sides of the flexible barrier are also symmetrical  
 350 when they are under a uniform impact pressure. Thus, the left post and its supporting  
 351 cables: Cable A Left and Cable B Left are selected as the analysis objects. The force  
 352 analysis of the supporting cables is divided into two steps:

353 Firstly, forces on Cable A Left and Cable B Left are decomposed into components in  
 354 the rotation plane of the post based on the top-view sketch (see Fig.14(a)):

$$355 \quad F_{AL,H} = F_{AL} \cdot \cos \alpha \quad (6)$$

$$356 \quad F_{BL,H} = F_{BL} \cdot \cos \beta \quad (7)$$

357 where  $F_{AL}$  and  $F_{BL}$  are the measured maximum tensile forces on Cable A Left and Cable  
 358 B Left during the impact,  $F_{AL,H}$  and  $F_{BL,H}$  are the components of  $F_{AL}$  and  $F_{BL}$   
 359 decomposed in the rotation plane of the left post, and  $\alpha$ ,  $\beta$  are the included angles  
 360 between Cable A, Cable B and the rotation plane of the post.

361

362 Secondly, based on the calculated  $F_{AL,H}$  and  $F_{BL,H}$ , components of the tensile forces on  
 363 Cable A Left and Cable B Left in the direction of impact can be calculated based on the  
 364 left-side-view sketch (see Fig.14 (b)):

$$365 \quad F_{AL,impact} = F_{AL,H} \cdot \cos \gamma \quad (8)$$

$$366 \quad F_{BL,impact} = F_{BL,H} \cdot \cos \delta \quad (9)$$



367 where  $F_{AL,impact}$  and  $F_{BL,impact}$  are the components of tensile forces on Cable A Left and  
 368 Cable B Left in the direction of impact, and  $\gamma$ ,  $\delta$  are the included angles between Cable  
 369 A, Cable B and the direction of impact.

370

371 It is defined that the direction of the supporting force, which is opposite to the direction  
 372 of the impact force, is the positive direction. Thus, the components of the tensile forces  
 373 on the left cables in the direction of impact ( $F_L$ ) can be calculated by substituting Eqs.  
 374 (6) and (7) into Eqs. (8) and (9):

$$375 \quad \begin{aligned} F_L = F_{BL,impact} - F_{AL,impact} &= F_{BL,H} \cdot \cos \delta - F_{AL,H} \cdot \cos \gamma \\ &= F_{BL} \cdot \cos \delta \cdot \cos \beta - F_{AL} \cdot \cos \gamma \cdot \cos \alpha \end{aligned} \quad (10)$$

376 Finally, based on the conservation of angular momentum and the symmetrical  
 377 arrangement of the cables and the posts with respect to the flexible barrier, the  
 378 equivalent impact force can be calculated from the tensile forces on the supporting  
 379 cables with the following equation:

$$380 \quad F_{Cables,equivalent} = \frac{l_{post}}{l_{impact}} [(F_{BL} + F_{BR}) \cdot \cos \delta \cdot \cos \beta - (F_{AL} + F_{AR}) \cdot \cos \gamma \cdot \cos \alpha] \quad (11)$$

381 where  $F_{Cables,equivalent}$  is the equivalent impact force calculated from the tensile forces on  
 382 the supporting cables,  $l_{post}$  is the distance between the rotation fulcrum of the post and  
 383 the connecting point of the cables,  $l_{impact}$  is the distance between the rotation fulcrum of  
 384 the post and the equivalent impact height of the granular flow.  $F_{AL}$ ,  $F_{AR}$ ,  $F_{BL}$ , and  $F_{BR}$   
 385 are the measured maximum tensile forces on the supporting cables. Their values are  
 386 presented in Fig.13. All parameters, as well as the calculated results, are listed in Table  
 387 2.

388

389 It is found that flexibility of flexible barriers makes an obvious contribution to the  
 390 reduction of the impact loading from a debris flow (Volkwein 2014; Song *et al.* 2017).  
 391 Since almost all the debris material was trapped in this study, the load reduction mainly  
 392 attributes to the large deformation of the flexible ring net during the impact. To quantify  
 393 the contribution of flexibility to impact loading reduction, the Loading Reduction Rate  
 394 (LRR) of the flexible barrier is defined as:

$$395 \quad LRR = \frac{F_{impact} - F_{Cables, equivalent}}{F_{impact}} \cdot 100\% \quad (12)$$

396 LRR in the granular flow tests is calculated and presented in Table 2. It is found that  
 397 around 28 % of the impact loading from the dry granular flow in Test 1 was attenuated  
 398 by the flexible barrier.

399

#### 400 ***4.3 Comparison of simple approaches with measured impact forces***

401 Two widely accepted simple approaches for impact force estimation: hydro-dynamic  
 402 approach and hydro-static approach (Kwan and Cheung 2012; Volkwein 2014; Song *et*  
 403 *al.* 2017; Ashwood and Hungr 2016; Wendeler 2008; Wendeler *et al.* 2018) are  
 404 compared in this section to validate their applications in the design of flexible barriers.

405 To quantify the accuracies of the simple approaches, Relative Error (RE) is usually  
 406 defined as:

$$407 \quad RE = \left| \frac{F_{calculated} - F_{measured}}{F_{measured}} \right| \times 100\% \quad (13)$$

408 where  $F_{calculated}$  represent the calculated impact force of the simple approach, which is  
 409 obtained by integrating the parameters listed in Table 1 and Table 2 into the hydro-  
 410 dynamic and hydro-static approaches listed in Table 3. [In the table, two dynamic](#)  
 411 [coefficients suggested by Wendeler \(2008\): 0.7 for mud flow and 2.0 for granular flow](#)

412 and a static coefficient of 1.0 are utilized.  $F_{measured}$  is the measured impact force on  
413 different components of the flexible barrier.

414 The calculated results are validated using the measured impact forces on the flexible  
415 ring net and on the supporting structures. The validation results are quantified with the  
416 value of Relative Error. The results of the calculation and the validation are listed in  
417 Table 3. Compared with the measured impact force on the flexible ring net directly, the  
418 hydro-dynamic approach with the dynamic coefficient of 2.0 has the best performance  
419 in estimating the impact force on the flexible ring net with a small deviation of 5.8 %,  
420 which verifies the dynamic coefficient suggested by Wendeler (2008) for granular  
421 flows. The reduced dynamic coefficient of 0.7 for debris flows with lower densities  
422 (lower than 1900 kg/m<sup>3</sup>), on the other hand, obviously under-estimated the loading on  
423 the flexible ring net by 50%. The reduction of the dynamic coefficient takes account of  
424 the dewatering and penetration of small particles during the impact based on lab tests  
425 and field observations (Wendeler 2008; Wendeler and Volkwein 2015; Wendeler *et al.*  
426 2018). Therefore, the under-estimation of the impact loading could attribute to the all  
427 trapped granular material by the secondary mesh net in our dry granular flow impact  
428 tests based on the observations of the impact process with the high-speed cameras.

429 While the hydro-static approach with the static coefficient of 1.0 fits quite well with the  
430 measured impact force on the supporting structures. This is reasonable since part of the  
431 dynamic impact from the granular flow can be attenuated by the flexible ring net, and  
432 the static loading can be fully transferred to the supporting structures. This phenomenon  
433 is also proved by the gradually increased tensile forces on Cable B Left and Cable B  
434 Right shown in Fig.13 (b). Thus, in the design of a flexible barrier for debris flow  
435 mitigation, the hydro-dynamic approach and the hydro-static approach can be used in  
436 the design and the selection of the flexible ring net and the supporting structures,

437 respectively. Even the dynamic coefficients and the static coefficient are verified by the  
438 data of large-scale tests in this study, more tests are required to further verify and select  
439 suitable coefficients before they can be used in the design.

440

## 441 **5. Conclusions**

442 In this paper, an improved large-scale physical modelling facility for debris flow  
443 research and a well-arranged high-frequency measurement system are introduced.  
444 Using this device, two tests were performed to study the behavior of a flexible barrier  
445 subjected to the impacts of granular flows. From the experimental data and their  
446 analysis, key findings and conclusions are summarized and presented as below:

447 (a) In Test 1, the front of the granular flow impacted the flexible ring net directly,  
448 deposited behind the barrier layer by layer, and formed a deposition wedge in the  
449 first second. After 1.0 s, the following granular flow deposited behind the  
450 deposition wedge.

451 (b) The static loading and the dynamic loading co-existed in the impact process, and  
452 the static loading was dominant. The static loading attributed to the gradual  
453 deposition of aggregate, and the dynamic loading was caused by the impact of the  
454 debris front. The latter arrived granular front applied impact loading on the flexible  
455 barrier via the deposition wedge. With the deposition of aggregate, the stationary  
456 debris formed a cushion behind the barrier and attenuated all the impact loading  
457 from the following granular front.

458 (c) In Test 2, the second granular flow in a multiple flow event was performed. The  
459 velocity and the flow depth of the granular flow decreased during movement, and  
460 the front stopped before it can reach the flexible barrier due to the large basal

461 friction between the moving granular flow and the granular deposition and the poor  
462 fluidity of the dry granular flow.

463 (d) The impact loading on a flexible ring net was directly measured from the tensile  
464 forces on the central area of the flexible ring net. In Test 1, the measured maximum  
465 impact force on the flexible ring net was 10.96 kN.

466 (e) The contribution of flexibility to impact loading reduction is quantified by  
467 introducing the Loading Reduction Rate (LRR). By calculating the impact loading  
468 transferred to the supporting structures, it can be concluded that almost 28 % of the  
469 impact loading from the granular flow was attenuated by the flexible ring net.

470 (f) From the comparisons of the hydro-dynamic approach and the hydro-static  
471 approach with the measured impact forces on different components, it is found that  
472 the hydro-dynamic approach with the dynamic coefficient of 2.0 fits well with the  
473 measured impact force on the flexible ring net, and the hydro-static approach with  
474 the static coefficient of 1.0 has a good performance in estimating the impact force  
475 on the supporting structures.

476

477 With the conclusions drawn from the large-scale tests in this paper, it can be found that  
478 the impact force on the flexible ring net and on the supporting structures are different  
479 due to the large deformation of the flexible ring net, thus the loadings on them should  
480 be estimated separately. By applying the LRR (Loading Reduction Rate) and suitable  
481 impact loading estimation approaches (see the verification results plotted in Table 3),  
482 the impact forces on the flexible ring net and on the supporting structures can be  
483 respectively estimated. Thus, the design of a flexible barrier for debris flow mitigation  
484 can be optimized by dimensioning and designing different components with different  
485 designed loadings, which provides a safer and more economical design method. In the

486 future, the tests of rapid debris flows will be conducted to investigate the behavior of  
487 debris flows and examine the performance of a flexible barrier under the impact of rapid  
488 debris flows.

489

#### 490 **Acknowledgement**

491 The authors acknowledge the financial support from Research Institute for Sustainable  
492 Urban Development of The Hong Kong Polytechnic University (PolyU). The work in  
493 this paper is also supported by a National State Key Project “973” grant (Grant No.:  
494 2014CB047000) (sub-project No. 2014CB047001) from Ministry of Science and  
495 Technology of the People’s Republic of China, a CRF project (Grant No.:  
496 PolyU12/CRF/13E) from Research Grants Council (RGC) of Hong Kong Special  
497 Administrative Region Government of China. The financial supports from PolyU  
498 grants (1-ZVCR, 1-ZVEH, 4-BCAU, 4-BCAW, 4-BCB1, 5-ZDAF) are acknowledged.  
499 This paper is also supported by Research Centre for Urban Hazards Mitigation of  
500 Faculty of Construction and Environment of PolyU.

501

#### 502 **References**

- 503 Arattano, M., and Marchi, L.: Measurements of debris flow velocity through cross-  
504 correlation of instrumentation data. *Natural Hazards and Earth System Science*,  
505 5(1), 137-142, 2005.
- 506 Armanini, A., and Michiue, M.: *Recent developments on debris flows* (Vol. 64).  
507 Springer, 1997.
- 508 Ashwood, W., and Hungr, O. Estimating total resisting force in flexible barrier  
509 impacted by a granular avalanche using physical and numerical modeling.  
510 *Canadian Geotechnical Journal*, 53(10), 1700-1717, 2016.

511 [ASTM, C. Standard test method for bulk density \(“unit weight”\) and voids in aggregate,](#)  
512 [2009.](#)

513 Berti, M., Genevois, R., Simoni, A. and Tecca, P.R. Field observations of a debris flow  
514 event in the Dolomites. *Geomorphology*, 29(3-4), 265-274, 1999.

515 Bugnion, L., McArdell, B. W., Bartelt, P., and Wendeler, C. Measurements of hillslope  
516 debris flow impact pressure on obstacles. *Landslides*, 9(2), 179-187, 2012.

517 Canelli, L., Ferrero, A. M., Migliazza, M., and Segalini, A. Debris flow risk mitigation  
518 by the means of rigid and flexible barriers-experimental tests and impact analysis.  
519 *Natural Hazards and Earth System Sciences*, 12(5), 1693, 2012.

520 Chen, H.X., Zhang, L.M., Gao, L., Yuan, Q., Lu, T., Xiang, B. and Zhuang, W.L.  
521 Simulation of interactions among multiple debris flows. *Landslides*, 14(2), 595-  
522 615, 2017.

523 Cui, P., Zeng, C. and Lei, Y. Experimental analysis on the impact force of viscous  
524 debris flow. *Earth Surface Processes and Landforms*, 40(12), 1644-1655, 2015.

525 DeNatale, J. S., Iverson, R. M., Major, J. J., LaHusen, R. G., Fiegel, G. L., and Duffy,  
526 J. D. Experimental testing of flexible barriers for containment of debris flows. US  
527 Department of the Interior, US Geological Survey, 1999.

528 Hungr, O. A model for the runout analysis of rapid flow slides, debris flows, and  
529 avalanches. *Canadian Geotechnical Journal*, 32(4), 610-623, 1995.

530 Hungr, O., Morgan, G.C., and Kellerhals, R. Quantitative Analysis of Debris Torrent  
531 Hazards for Design of Remedial Measures. *Canadian Geotechnical Journal* 21(4):  
532 663–77, 1984.

533 Hutter, K. and Koch, T. Motion of a granular avalanche in an exponentially curved  
534 chute: experiments and theoretical predictions. *Phil. Trans. R. Soc. Lond. A*,  
535 334(1633), 93-138, 1991.

536 Ishikawa, N., Inoue, R., Hayashi, K., Hasegawa, Y., and Mizuyama, T. Experimental  
537 approach on measurement of impulsive fluid force using debris flow model. *na*,  
538 2008.

539 Iverson, R.M., Logan, M., LaHusen, R.G. and Berti, M. The perfect debris flow?  
540 Aggregated results from 28 large-scale experiments. *Journal of Geophysical*  
541 *Research: Earth Surface*, 115(F3), 2010.

542 Iverson, R.M. Scaling and design of landslide and debris-flow experiments.  
543 *Geomorphology*, 244, 9-20, 2015.

544 Kwan J.S.H. and Cheung R.W.M. Suggestions on design approaches for flexible  
545 debris-resisting barriers. Discussion Note No. DN 1/2012, Geotechnical  
546 Engineering Office, Hong Kong, 90, 2012.

547 Kwan, J.S.H., Chan, S.L., Cheuk, J.C.Y. and Koo, R.C.H. A case study on an open  
548 hillside landslide impacting on a flexible rockfall barrier at Jordan Valley, Hong  
549 Kong. *Landslides*, 11(6), 1037-1050, 2014.

550 Lichtenhahn, C. Die Berechnung von Sperren in Beton und Eisenbeton [Die design of  
551 barriers made of concrete and reinforced concrete]. *Kolloquium u`ber*  
552 *Wildbachsperren*. *Mitteilungen der Forstlichen Bundesanstalt Wien*. Heft, 102, 91-  
553 127. (in German), 1973.

554 Miura, K., Maeda, K. and Toki, S. Method of measurement for the angle of repose of  
555 sands. *Soils and Foundations*, 37(2), 89-96, 1997.

556 Paik, J., Son, S., Kim, T., and Kim, S. A real-scale field experiment of debris flow for  
557 investigating its deposition and entrainment. In *AGU Fall Meeting Abstracts*, 2012.

558 Prochaska, A.B., Santi, P.M., Higgins, J.D. and Cannon, S.H. A study of methods to  
559 estimate debris flow velocity. *Landslides*, 5(4), 431-444, 2008.

560 Rankine, W. On the stability of loose earth. *Philosophical Transactions of the Royal*  
561 *Society of London*, Vol. 147, 9-27, 1857.

562 Santi, P. M., Hewitt, K., VanDine, D. F., and Cruz, E. B. Debris-flow impact,  
563 vulnerability, and response. *Natural hazards*, 56(1), 371-402, 2011.

564 Song, D., Choi, C. E., Ng, C. W. W., and Zhou, G. G. D. Geophysical flows impacting  
565 a flexible barrier: effects of solid-fluid interaction. *Landslides*, 1-12, 2017.



566 Su, L.J., Xu, X.Q., Geng, X.Y. and Liang, S.Q. An integrated geophysical approach for  
567 investigating hydro-geological characteristics of a debris landslide in the  
568 Wenchuan earthquake area. *Engineering Geology*, 219, 52-63, 2017.

569 Takahashi, T. Debris flow: mechanics, prediction and countermeasures. CRC press,  
570 2014.

571 Volkwein, A. Flexible debris flow barriers. Design and application. WSL Berichte.  
572 Issue 18, 29, 2014.

573 Volkwein, A., Wendeler, C., and Guasti, G. Design of flexible debris flow barriers. In  
574 5th International Conference debris-flow hazard mitigation. Mechanics, prediction  
575 and assessment. Padua, Italy 1093-1100, 2011.

576 Wendeler, C. S. I. Murgangrückhalt in Wildbächen. Grundlagen zu Planung und  
577 Berechnung von flexiblen Barrieren. ETH, 2008.

578 Wendeler, C., and Volkwein, A. Laboratory tests for the optimization of mesh size for  
579 flexible debris-flow barriers. *Natural Hazards and Earth System Sciences*, 15(12),  
580 2015.

581 Wendeler, C., McArdell, B. W., Rickenmann, D., Volkwein, A., Roth, A., and Denk,  
582 M. Field testing and numerical modeling of flexible debris flow barriers. In  
583 Proceedings of international conference on physical modelling in geotechnics,  
584 Hong Kong, 2006.

585 [Wendeler, C., Volkwein, A., McArdell, B.W. and Bartelt, P. Load model for designing](#)  
586 [flexible steel barriers for debris flow mitigation. \*Canadian Geotechnical Journal\*,](#)  
587 [\(ja\), 2018.](#)

588 Wendeler, C., Volkwein, A., Roth, A., Denk, M., and Wartmann, S. Field  
589 measurements and numerical modelling of flexible debris flow barriers. *Debris-*  
590 *Flow Hazards Mitig. Mech. Predict. Assess.* Millpress, Rotterdam, 681-687, 2007.

591 WSL. Report on testing SL-100 a protection system against shallow landslides, 2010.

592 Xu, Q., Zhang, S., Li, W.L. and Van Asch, T.W. The 13 August 2010 catastrophic  
593 debris flows after the 2008 Wenchuan earthquake, China. *Natural Hazards and*  
594 *Earth System Sciences*, 12, 201-216, 2012.

- 595 Yagi, H., Sato, G., Higaki, D., Yamamoto, M., and Yamasaki, T. Distribution and  
596 characteristics of landslides induced by the Iwate–Miyagi Nairiku earthquake in  
597 2008 in Tohoku District, Northeast Japan. *Landslides* 6(4):335–344, 2009.
- 598 Zhou, G.G., Ng, C.W., and Sun, Q.C. A new theoretical method for analyzing confined  
599 dry granular flows. *Landslides*, 11(3), 369-384, 2014.

## Tables

**Table 1.** Main properties of aggregate used in the test

Main properties	Values
<i>The total volume of aggregate in Test 1 and Test 2 (m<sup>3</sup>)</i>	4
<i>Particle diameters (mm)</i>	15 ~ 30
<i>Internal friction angle (°)</i>	36
<i>Interface friction angle (°) (between aggregate and painted steel plate)</i>	28
<i>Bulk density (kg/m<sup>3</sup>)</i>	1600

**Table 2.** Values of measured parameters and calculated results in Test 1

Parameters and results	Values
<i>Moving speed (m/s)</i>	5
<i>Included angle <math>\theta</math> (<math>^{\circ}</math>)</i>	130
<i>A<sub>measured</sub> (m<sup>2</sup>)</i>	0.644
<i>A<sub>impact</sub> (m<sup>2</sup>)</i>	1.44
$\sum_{i=1}^{i=n} F_{tensile,i}$ (kN)	11.59
<i>F<sub>measured</sub> (kN)</i>	4.9
<i>l<sub>impact</sub> (m)</i>	0.242
<i>l<sub>post</sub> (m)</i>	2.7
<i>h<sub>debris</sub> (m)</i>	0.086
<i>h<sub>deposit</sub> (m)</i>	0.58
$\alpha$ ( $^{\circ}$ )	62
$\beta$ ( $^{\circ}$ )	24
$\gamma$ ( $^{\circ}$ )	76
$\delta$ ( $^{\circ}$ )	60
<i>F<sub>AL</sub> (kN)</i>	0.062
<i>F<sub>AR</sub> (kN)</i>	0.062
<i>F<sub>BL</sub> (kN)</i>	0.79
<i>F<sub>BR</sub> (kN)</i>	0.79
<i>F<sub>Cables, equivalent</sub> (kN)</i>	7.89
<i>F<sub>impact</sub> (kN)</i>	10.96
<i>Loading Reduction Rate (LRR) (%)</i>	28.01

**Table 3.** Comparisons of the calculated impact forces using simple approaches with the measured impact forces on different components of a flexible barrier in Test 1

Simple approaches for impact force estimation	Calculated impact force (kN)	RE with impact force on the flexible net (%)	RE with impact force on the supporting structures (%)
		$F_{impact}=10.96$ kN	$F_{Cables, equivalent} =7.89$ kN
$F_{calculated} = \alpha \rho_{bulk} v_0^2 h w$ <i>(hydro-dynamic approach with <math>\alpha=0.7</math>)</i> <i>(for muddy debris flows with lower densities)</i> <i>(Wendeler 2008)</i>	3.61	67.1	54.3
$F_{calculated} = \alpha \rho_{bulk} v_0^2 h w$ <i>(hydro-dynamic approach with <math>\alpha=2</math>)</i> <i>(for granular flows)</i> <i>(Wendeler 2008)</i>	10.32	<b>5.8</b>	30
$F_{calculated} = \kappa \rho_{bulk} g h_{deposit}^2 w$ <i>(hydro-static approach with <math>\kappa=1</math>)</i> <i>(Kwan and Cheung 2012)</i>	7.92	27.7	<b>0.38</b>

## Figure lists

**Figure 1.** (a) side view of a large-scale physical model design (unit in mm) and (b) photograph of the physical modelling facility constructed at a site in Hong Kong

**Figure 2.** Calibration of a tension link transducer

**Figure 3.** (a) schematic diagram of a flexible barrier and (b) front view of the flexible barrier with numbered tension link transducers between rings and the measured area in the physical model (unit in m)

**Figure 4.** Aggregate samples in the granular flow impact tests (unit in mm)

**Figure 5.** Side profiles of deposited aggregate at different times in Test 1

**Figure 6.** Relation between the deposition height of the granular flow, horizontal deformation of the flexible barrier and tensile force of Transducer 1 *v.s.* time in Test 1

**Figure 7.** Recorded forces *v.s.* time by the mini tension link transducers between rings in Test 1

**Figure 8.** Interpretation of the typical video frames in Test 1 recorded by (a) the side-view camera and (b) the front-view camera with the data of tensile force from Transducer 1

**Figure 9.** Motion of the granular flow in Test 2

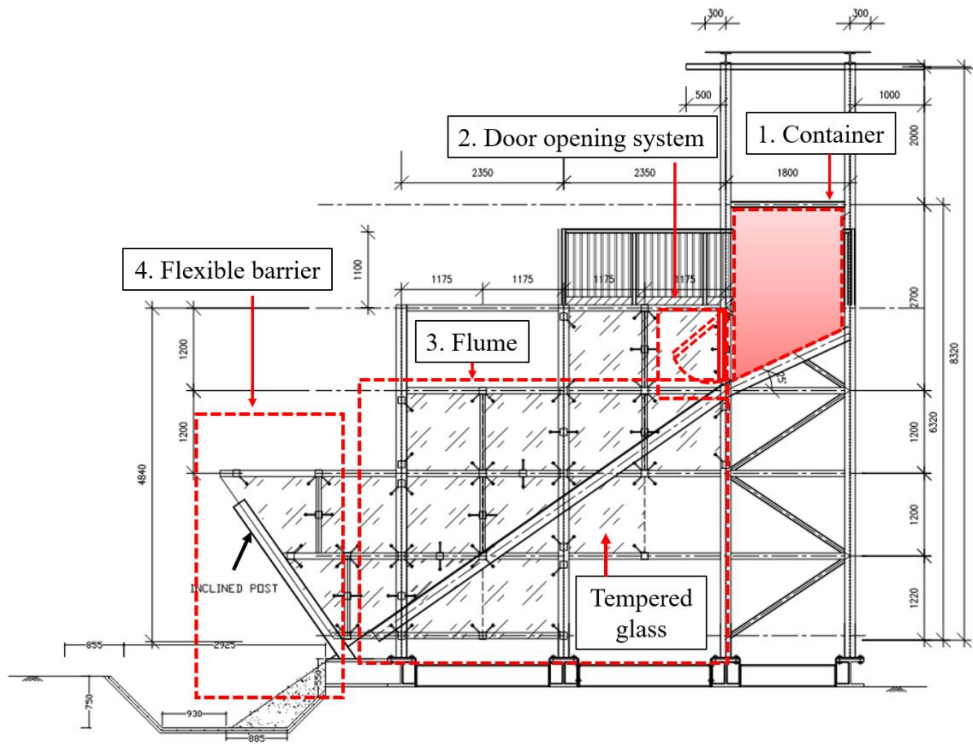
**Figure 10.** Side profile of the depositions in Test 1 and Test 2 and the velocity change of the granular flow in Test 2 with the moving distance

**Figure 11.** (a) sketch of the flexible barrier under the impact of a granular flow and (b) the simplified force analysis of the measured area in the cross-section of Transducer  $i$  and Transducer  $i+1$

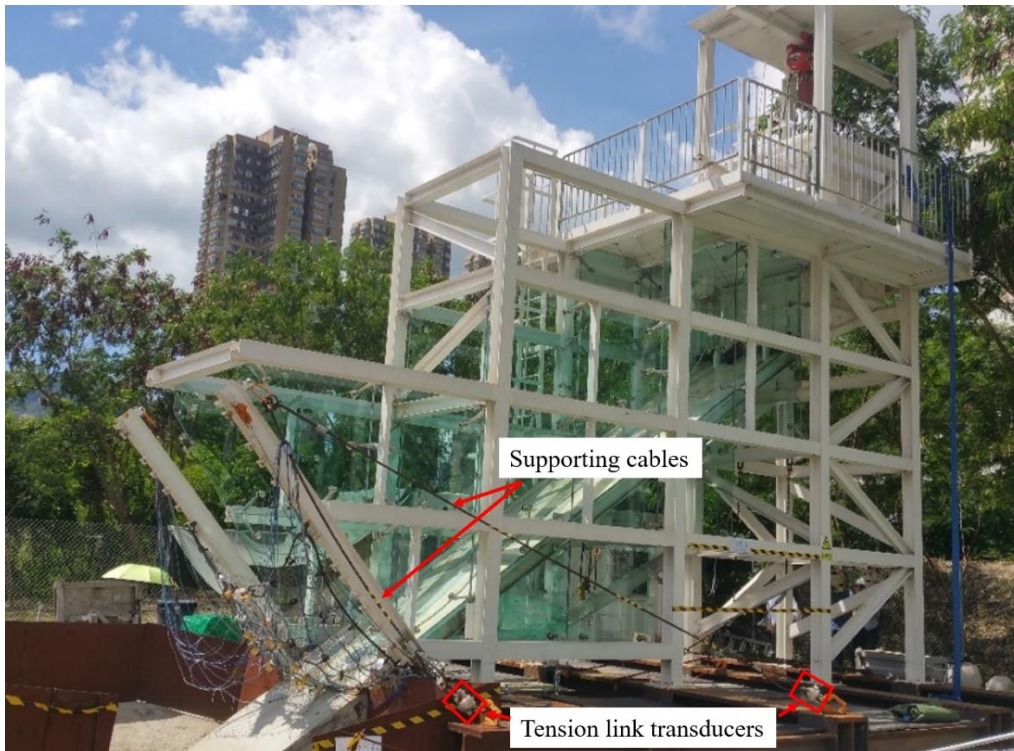
**Figure 12.** Sketch of the impact and measured area in Test 1 and the maximum tensile forces measured from 10 mini tension link transducers under the impact of the granular flow (unit in m)

**Figure 13.** (a) photograph at the instant of the largest deformation with measured parameters and (b) recorded forces and time by the tension link transducers on the supporting cables in Test 1

**Figure 14.** (a) top-view and (b) left-side-view of sketches with the force analysis of the posts and cables



(a)



(b)

**Figure 1.** (a) side view of a large-scale physical model design (unit in mm) and (b) photograph of the physical modelling facility constructed at a site in Hong Kong

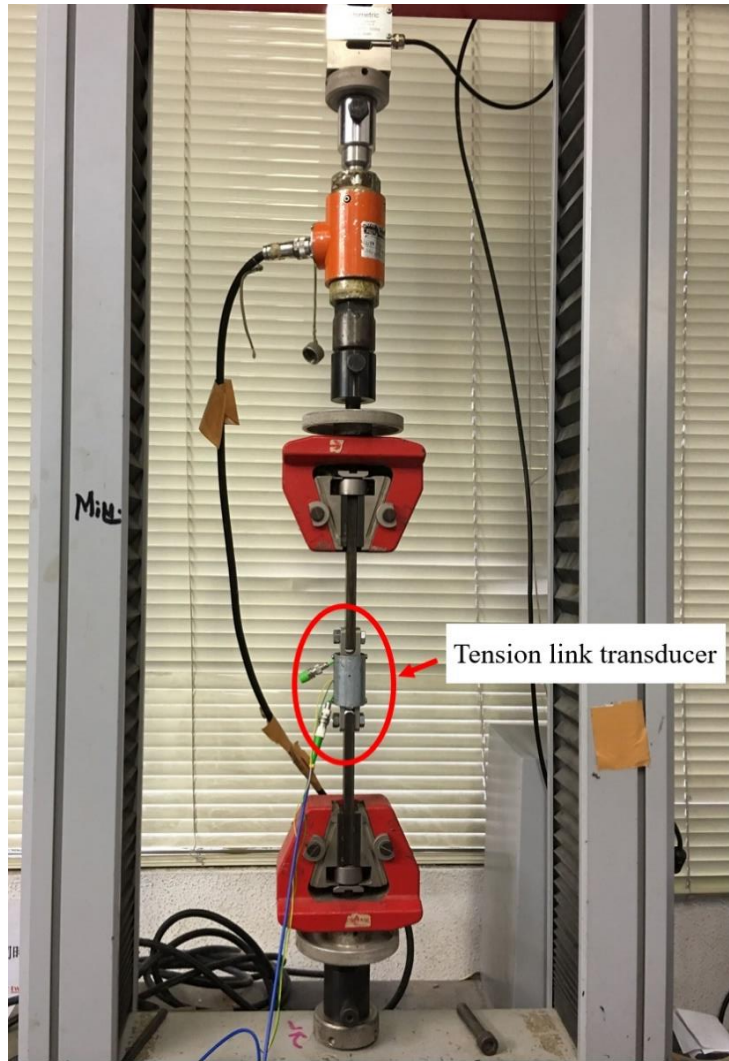
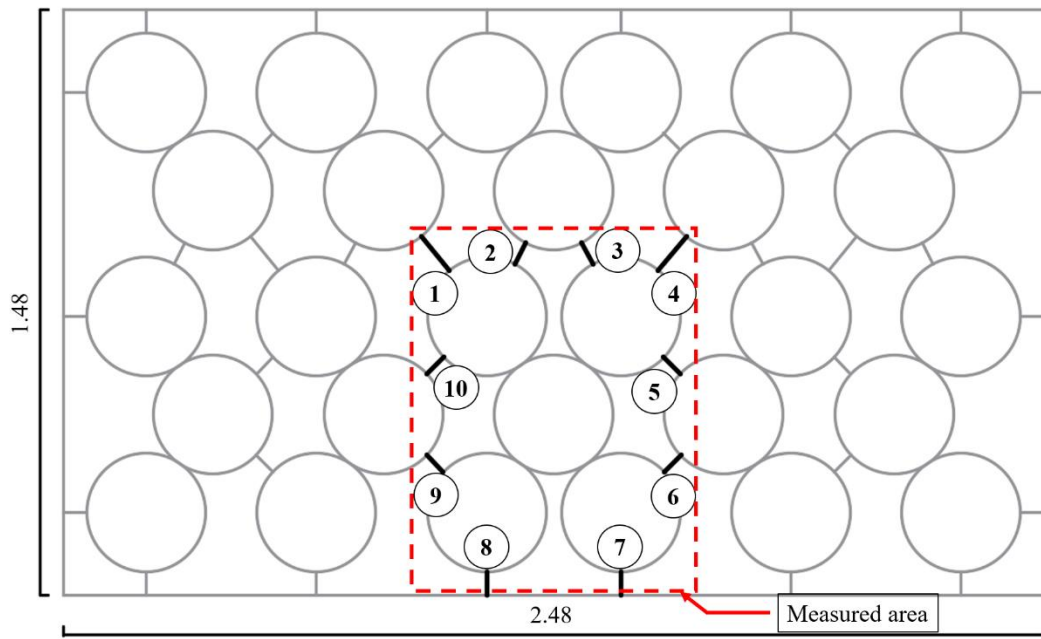
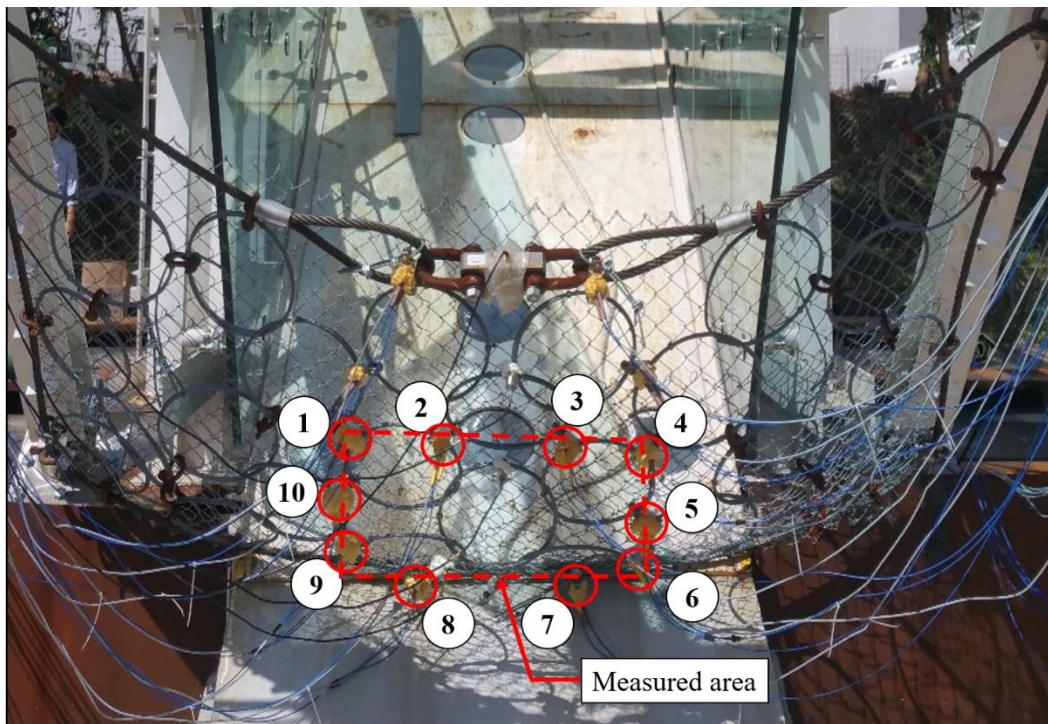


**Figure 2.** Calibration of a tension link transducer





(a)



(b)

**Figure 3.** (a) schematic diagram of a flexible barrier and (b) front view of the flexible barrier with numbered tension link transducers between rings and the measured area in the physical model (unit in m)



**Figure 4.** Aggregate samples in the granular flow impact tests (unit in mm)

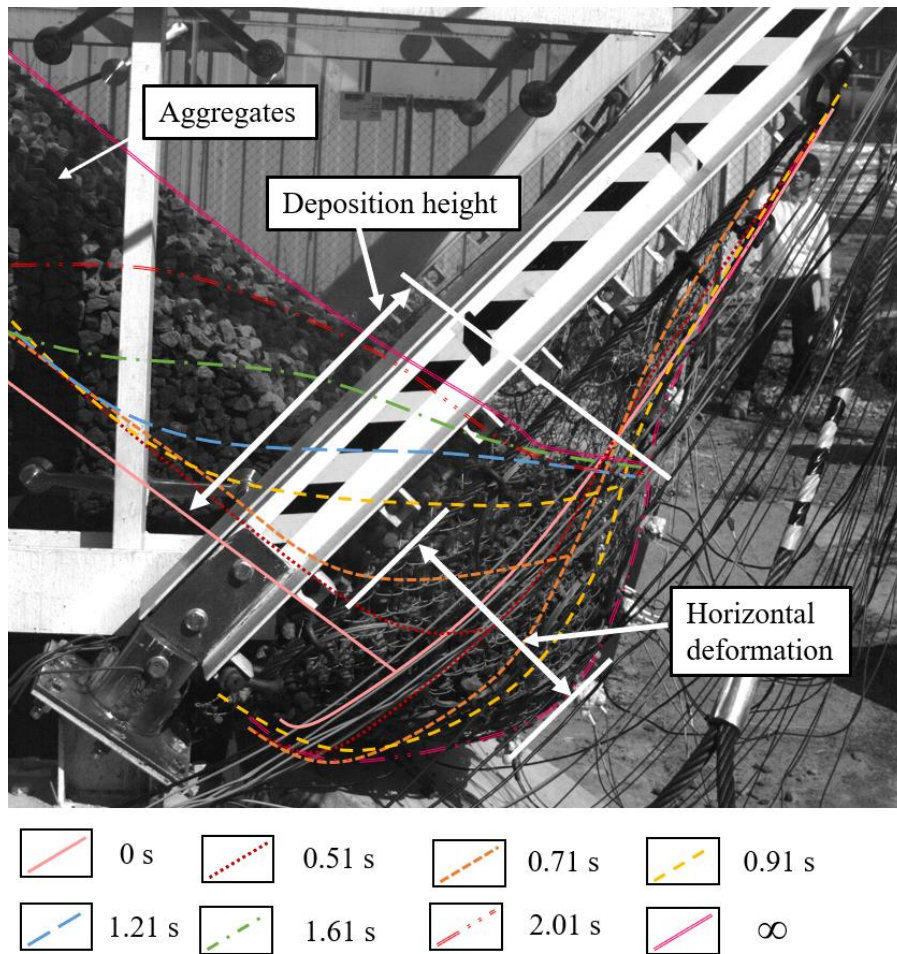


**Figure 5.** Side profiles of deposited aggregate at different times in Test 1

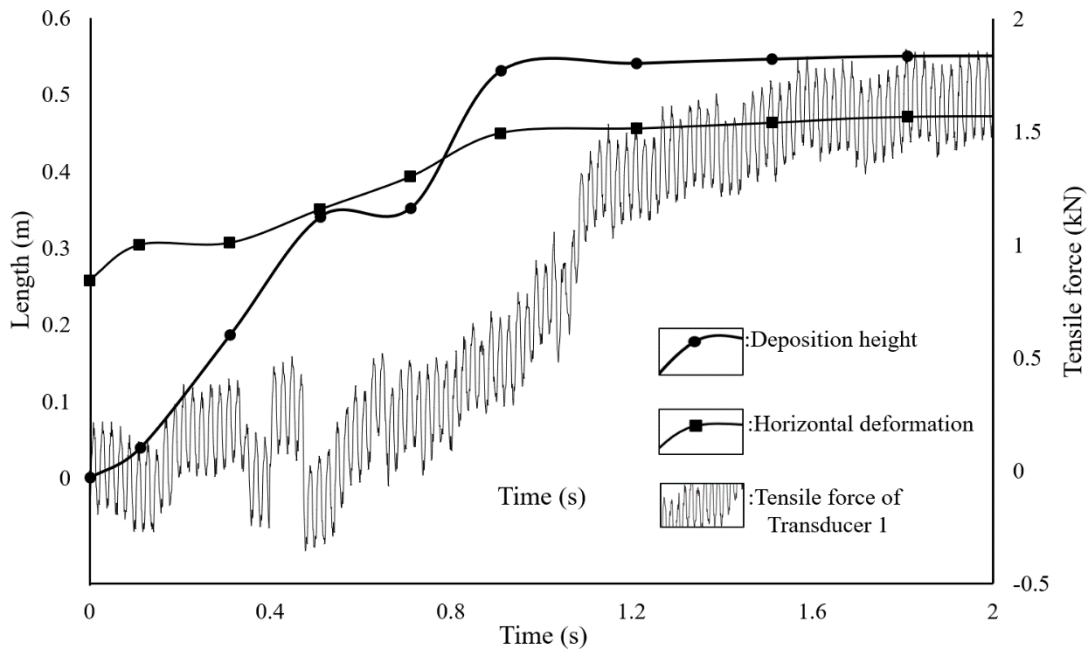


**Figure 6.** Relation between the deposition height of the granular flow, horizontal deformation of the flexible barrier and tensile force of Transducer 1 v.s. time in Test 1

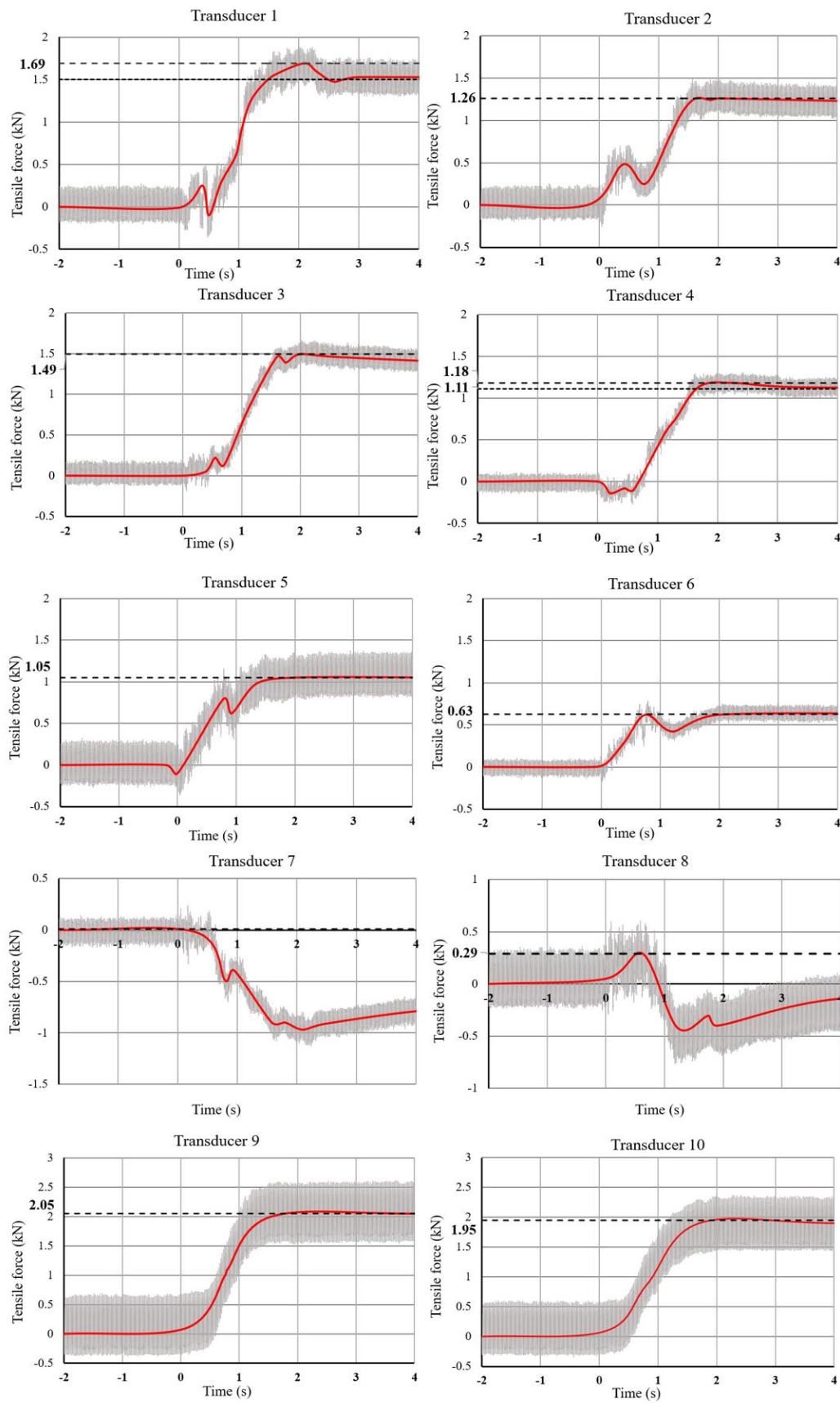
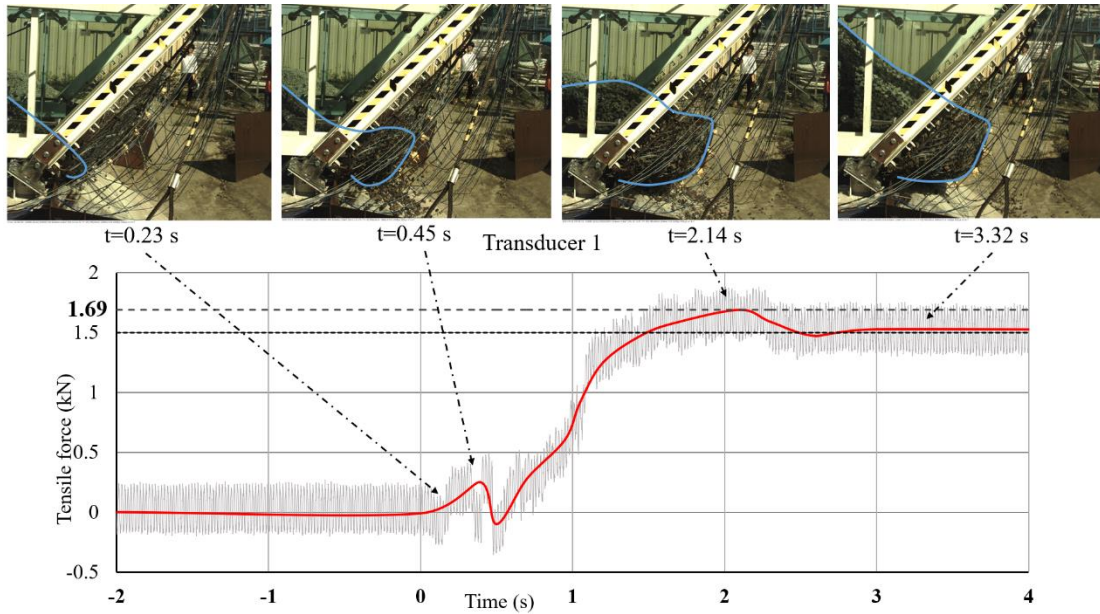
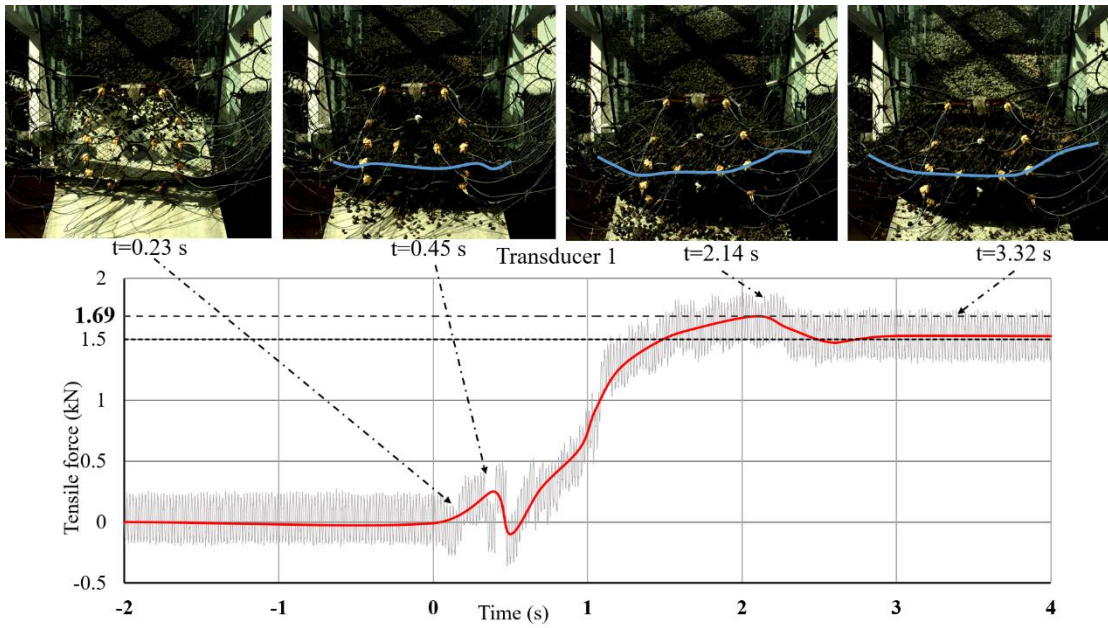


**Figure 7.** Recorded forces *v.s.* time by the mini tension link transducers between rings in Test 1



(a)



(b)

**Figure 8.** Interpretation of the typical video frames in Test 1 recorded by (a) the side-view camera and (b) the front-view camera with the data of tensile force from Transducer 1

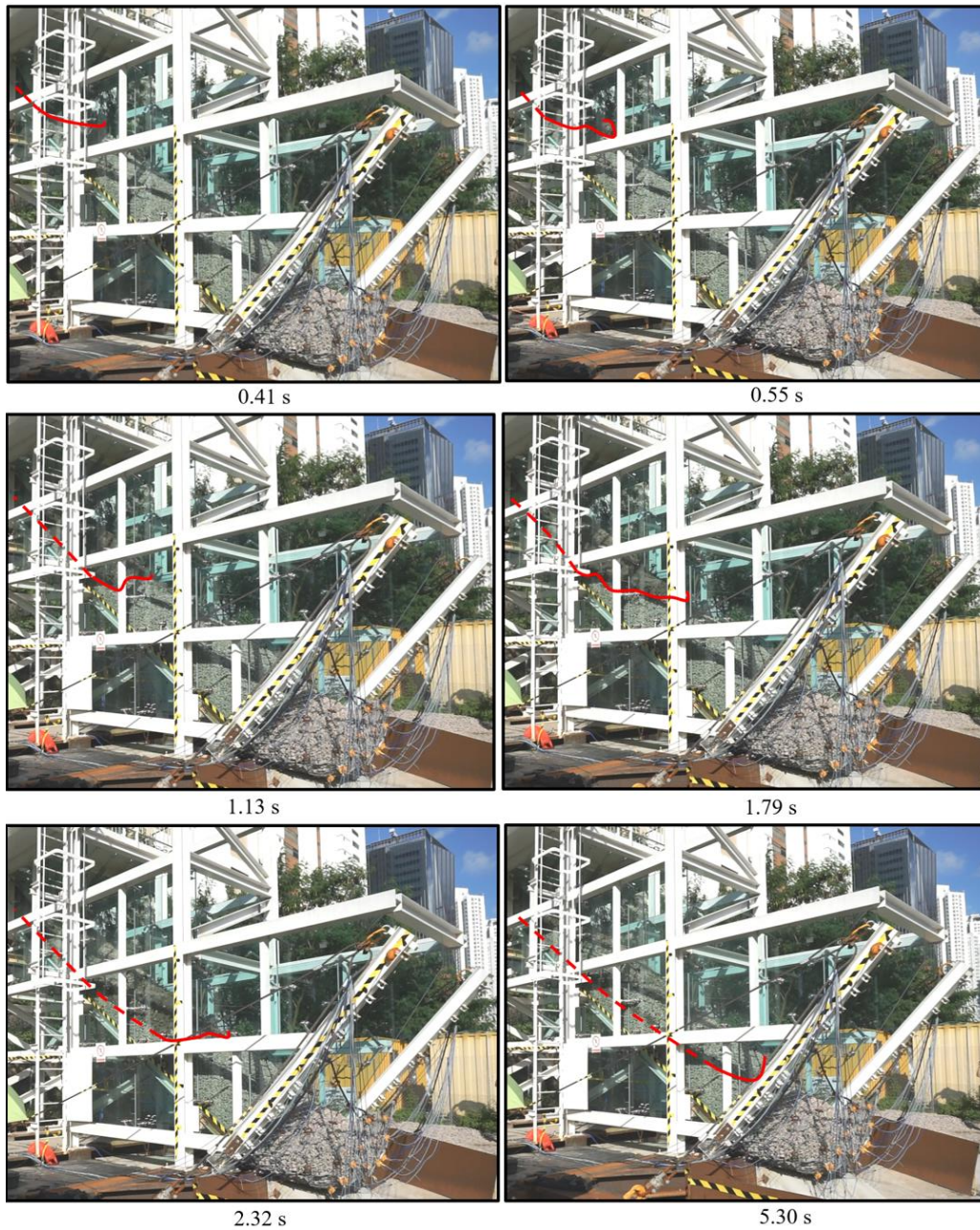


**Figure 9.** Motion of the granular flow in Test 2

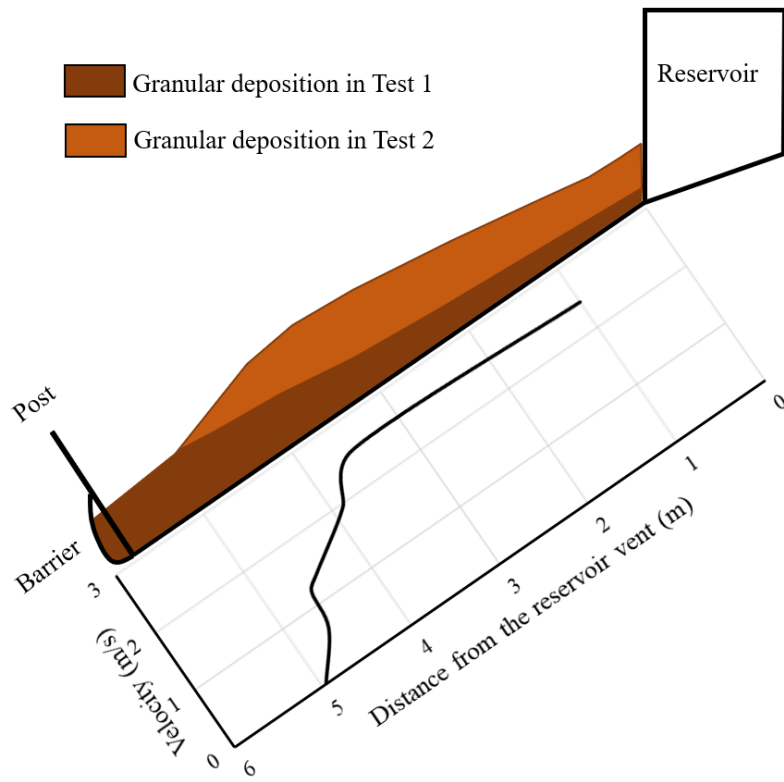


**Figure 10.** Side profile of the depositions in Test 1 and Test 2 and the velocity change of the granular flow in Test 2 with the moving distance



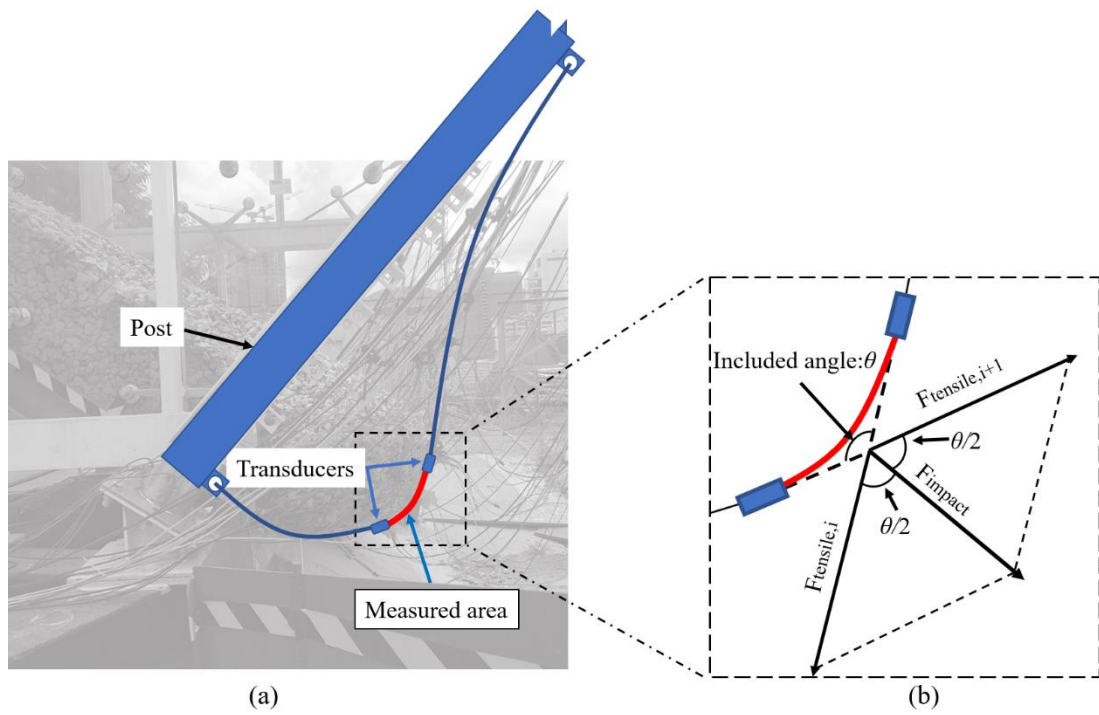


**Figure 11.** (a) sketch of the flexible barrier under the impact of a granular flow and (b) the simplified force analysis of the measured area in the cross-section of Transducer  $i$  and Transducer  $i+1$

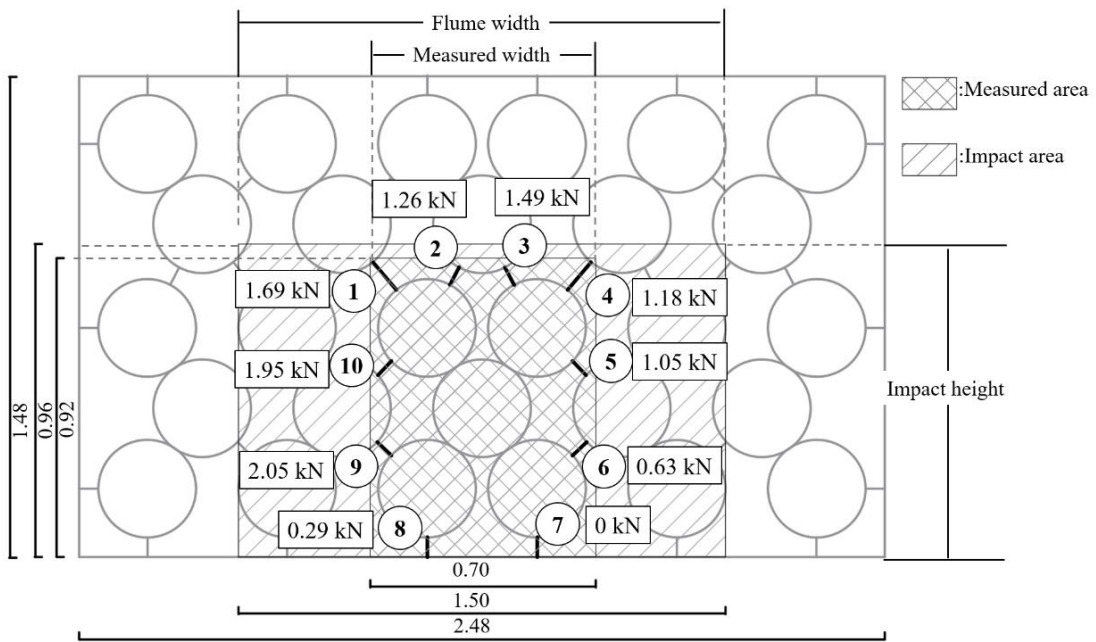
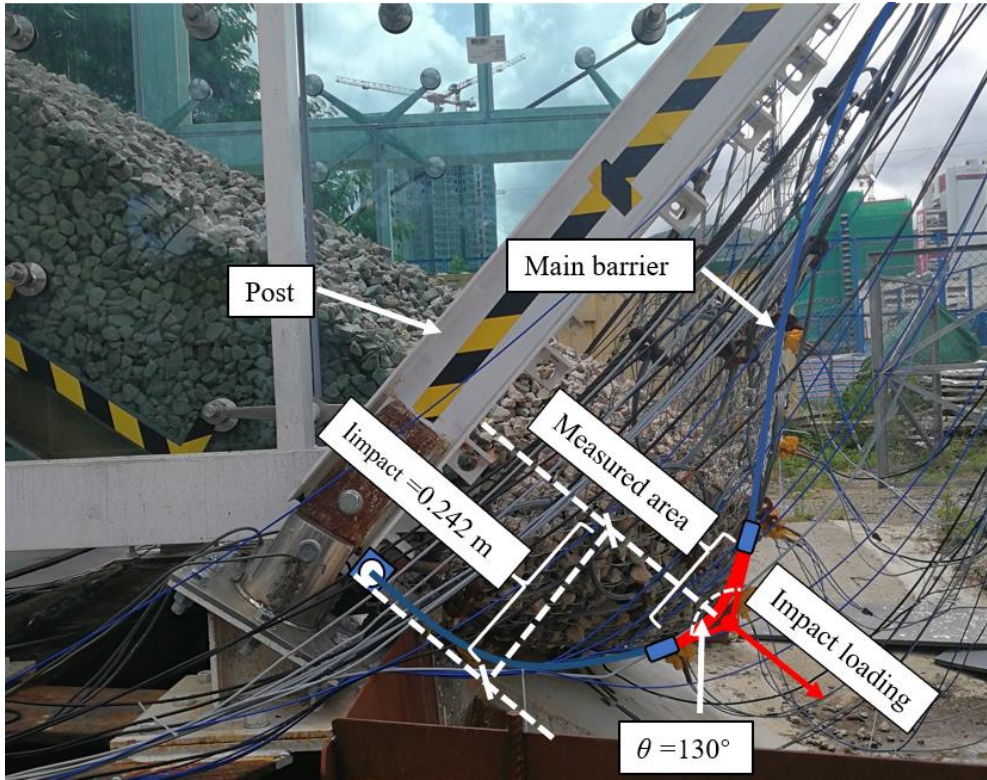
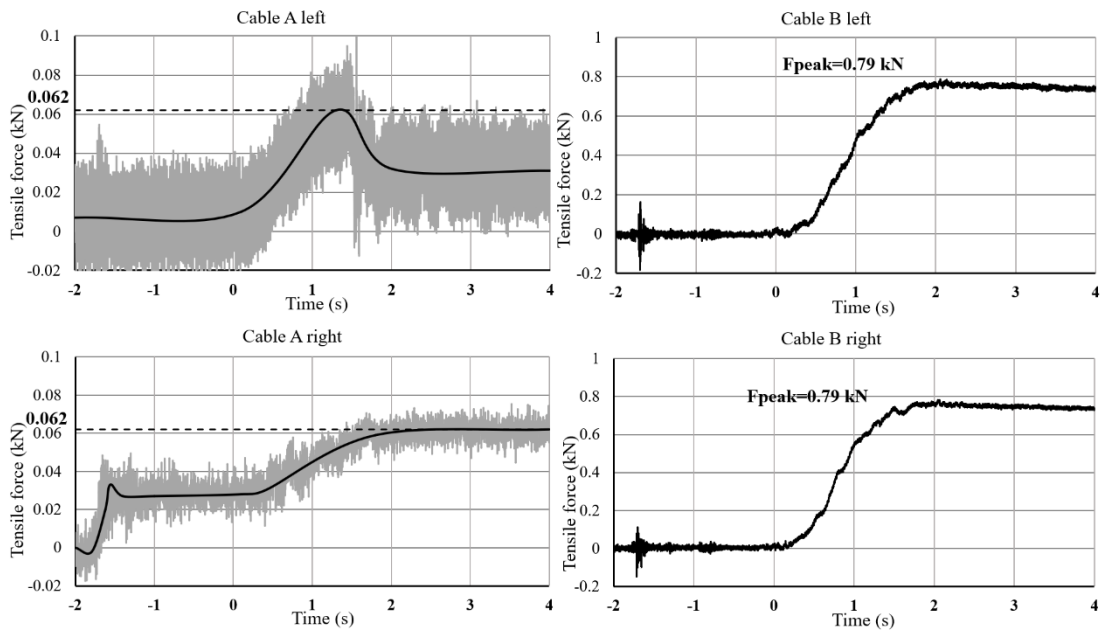


**Figure 12.** Sketch of the impact and measured area in Test 1 and the maximum tensile forces measured from 10 mini tension link transducers under the impact of the granular flow (unit in m)

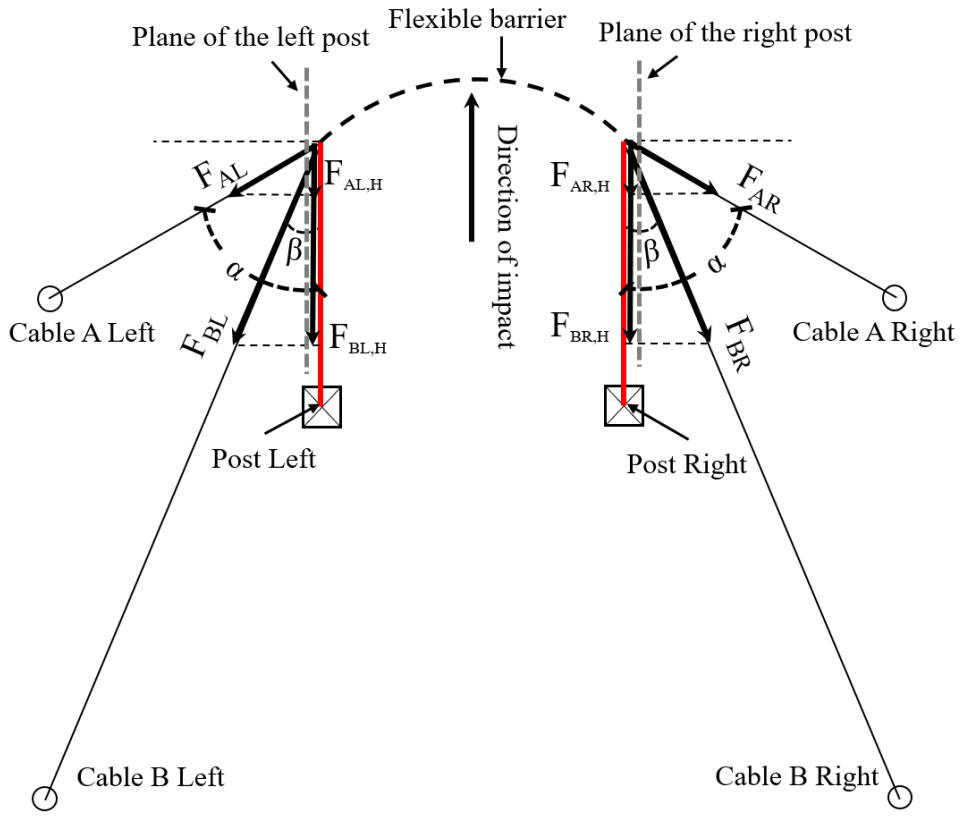


(a)

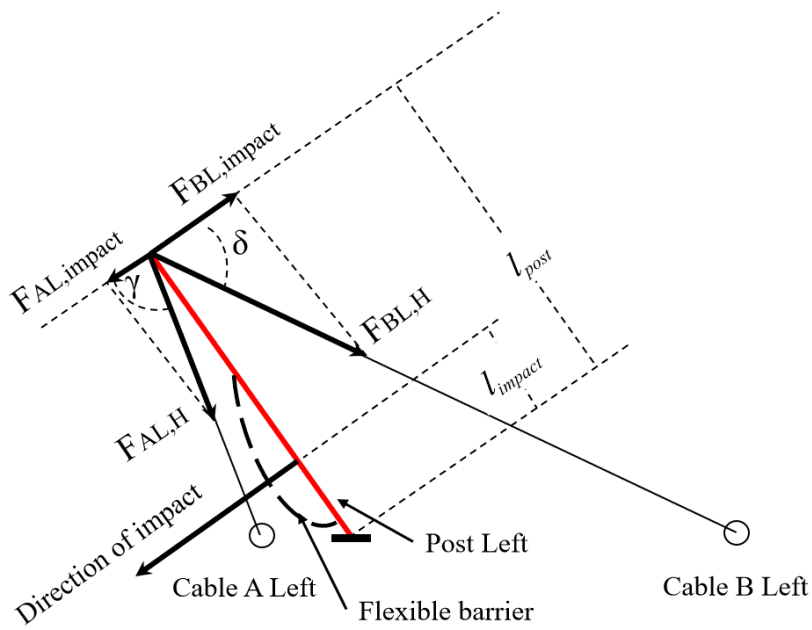


(b)

**Figure 13.** (a) photograph at the instant of the largest deformation with measured parameters and (b) recorded forces and time by the tension link transducers on the supporting cables in Test 1



(a)



(b)

**Figure 14.** (a) top-view and (b) left-side-view of sketches with the force analysis of the posts and cables